ARTICLE IN PRESS

Computers and Mathematics with Applications ▮ (▮▮▮▮) ▮▮▮–▮▮▮

Contents lists available at ScienceDirect

Computers and Mathematics with Applications

journal homepage: www.elsevier.com/locate/camwa

The role of the kinetic parameter in the stability of two-relaxation-time advection–diffusion lattice Boltzmann schemes

A. Kuzmin [a], I. Ginzburg [b,*], A.A. Mohamad [a]

[a] Mechanical and Manufacturing Engineering, Schulich School of Engineering, University of Calgary, Calgary, T2N 1N4 Alberta, Canada
[b] Cemagref, Antony Regional Centre, HBAN, Parc de Tourvoie BP 44, 92163 Antony Cedex, France

ARTICLE INFO

Keywords:
Lattice Boltzmann schemes
Anisotropic advection–diffusion equation
von Neumann stability analysis
Numerical diffusion
TRT
BGK

ABSTRACT

In general, explicit numerical schemes are only conditionally stable. A particularity of lattice Boltzmann multiple-relaxation-time (MRT) schemes is the presence of free ("kinetic") relaxation parameters. They do not appear in the transport coefficients of the modelled second-order (macroscopic) equations but they have an impact on the effective accuracy and stability of the algorithm. The simplest uniform choice (the well known BGK/SRT model) is often inadequate, and therefore a compromise in the complexity of the model is sought. For this purpose, the von Neumann stability analysis is performed for the d1Q3 two-relaxation-time (TRT) advection–diffusion model. The extended optimal (EOTRT) model, which relates the two collision times such that the most stable scheme is set by a suitable choice of the equilibrium parameters, equal for any Peclet number, is then developed. This extends the very recently derived optimal subclass (OTRT) to larger combinations of "physical" and "kinetic" collision rates. Next, we provide the necessary and/or sufficient stability limits on the EOTRT subclass for a wide range of velocity sets, with and without numerical diffusion, and delineate the interesting choices of free equilibrium weights for the d2Q9 and d3Q15 models. The BGK/SRT model is without advanced advection properties; we prove (for minimal stencil schemes d1Q3, d2Q5 and d3Q7) that the non-negativity of the equilibrium distribution is necessary for its stability in the advection-dominated limit. Beyond the EOTRT and BGK/SRT subclasses of the TRT model, blind choices of the "ghost" collision number may result in quite unstable schemes, even for positive equilibrium. However, we find that the d1Q3 stability curves govern the advection properties of the multi-dimensional models and a fuller picture of the TRT stability properties begins to emerge.

1. Introduction

There is a well established hierarchy of linear lattice Boltzmann relaxation operators for both hydrodynamic and anisotropic advection–diffusion equations (AADE); from the minimal single-relaxation-time BGK operator [1] to the richest ancestor: multiple-relaxation-time MRT operators [2–5], via the two-relaxation-time (TRT) operator [6,7]. A MRT operator offers d independent relaxation rates for d anisotropic diagonal components of the diffusion tensor, against only one available for the BGK and TRT operators. The alternative linkwise operators, the BGK-type operator [8,9] and the L-operator [6,10] with, respectively, one and two relaxation rates per velocity axis (called links), offer a number of independent times equal to the number of links for describing the full anisotropic tensors with the cross-diagonal diffusion elements. Since

* Corresponding author. Tel.: +33 1 40966060; fax: +33 1 40966270.
E-mail addresses: shurik.kuzmin@gmail.com (A. Kuzmin), irina.ginzburg@cemagref.fr (I. Ginzburg), mohamad@ucalgary.ca (A.A. Mohamad).

0898-1221/$ – see front matter © 2010 Elsevier Ltd. All rights reserved.
doi:10.1016/j.camwa.2010.07.036

BGK ∈ TRT ∈ MRT and BGK ∈ TRT ∈ L, the TRT operator is the largest common subclass of the MRT and L operators. The BGK and TRT models can also solve the AADE, but only with the help of *anisotropic* equilibrium distributions [6,11,12]. Of course, any practitioner will give a preference to a more conceptually complicated operator only if this "complexity" is justified, even when the two operators have the same computational cost as the BGK and TRT. To date there has been some evidence, e.g., in the works [5,13,14], of the possible gain in stability coming from "ghost" or "kinetic" relaxation times, but the whole scenario is not well understood, even for the simplest linear isotropic one-dimensional advection–diffusion equation. This is the main subject of this paper.

Before focusing on the technical details of the von Neumann stability analysis of the TRT model, let us summarize the results on the known role of its free collision number. Let $\tau^{\pm} = \frac{1}{2} + \Lambda^{\pm}$ be relaxation rates of the symmetric ("+") and anti-symmetric ("−") non-equilibrium components. Two analytical approaches, the infinite Chapman–Enskog expansion [15] and the recurrence equations [16], show that any *non-dimensional steady state solution* of the TRT model is *consistent* in the sense that it is *exactly* controlled by non-dimensional physical numbers (such as the Reynolds or Peclet numbers) only if a specific combination of the two relaxation times, the so called magic (free) parameter $\Lambda = \Lambda^{+}\Lambda^{-}$, is set for a given problem. As the simplest example, the inconsistency of the BGK model ($\tau = \tau^{\pm}$), formally beyond second order, results in quite unexpected *non-linear* behaviour of the steady solutions to the Stokes equation or linear ADE obtained when, respectively, Λ^{+} varies with the viscosity or Λ^{-} varies with the diffusion coefficients.

The control of steady solutions by Λ results in several particular choices which eliminate, e.g., the third-order ($\Lambda = \frac{1}{12}$) or the fourth-order ($\Lambda = \frac{1}{6}$) spatial errors [15,17]. Then the Λ interposes for the effective second-order accurate location of boundaries and interfaces. Only some boundary schemes retain the consistency of bulk solutions [18], like the bounce-back and anti-bounce-back reflexions: they locate the Dirichlet boundary values of anti-symmetric/symmetric equilibrium components, respectively, midway between the lattice nodes when, typically, $\Lambda = \frac{3}{16}$. The control over bulk and boundary accuracy is difficult for the BGK operator, especially when τ varies in space and time (two-phase problems, non-linear diffusion equations, etc), because of the unavoidable variation of $\Lambda = (\tau - \frac{1}{2})^2$. The purpose of this study is to establish the role of Λ in the stability of the TRT operator.

The von Neumann stability analysis may provide precise, necessary and sufficient (in periodic subdomains), stability conditions for linear LBE models, i.e., when the equilibrium is a linear function of the populations. The sufficient stability conditions need to estimate (in functions of the equilibrium parameters like velocity $\vec{U}$) whether the amplitudes of all Q roots of the Qth-order characteristic (polynomial) equation belong to interval [0, 1] for any possible orientation of wavevectors and velocity vectors. So far, very few exact solutions have been reported: Rheinländer [19] proves that the d1Q2 BGK ADE model remains stable for $|U| = 1$, and Suga [20] delineates the suitable velocity range, e.g., for one possible equilibrium of the d2Q9 BGK model but only when $\tau = 1$. The second-order numerical diffusion of the scheme is not taken into consideration in either publication. Recent results of a *numerical von Neumann analysis* by Servan-Camas and Tsai [21] indicate that the stability of the d1Q3 and multi-dimensional BGK ADE models (with and without numerical diffusion) decays when $\tau \to \frac{1}{2}$, i.e., in the advection-dominant limit, towards the non-negativity domain where the equilibrium functions (divided by the conserved quantity) are all non-negative. At the same time, their numerical study [22] of the TRT operator illustrates the impact, both "positive" and "negative", of the free "kinetic" relaxation rate on the stable velocity amplitude. However, any discrete (numerical) study would meet difficulties in finding the most stable or unreliable solutions for a "kinetic" collision rate.

One interesting solution for the TRT mass conserving models has been recently described [23]: when $\Lambda = \frac{1}{4}$. This choice delineates for all velocity sets the so-called (optimal) OTRT subclass. The OTRT subclass is "unconditionally" stable in the sense that it may provide stable solutions for *any grid Peclet number with the same values for all equilibrium parameters*. In fact, the TRT characteristic equation admits the same equilibrium stability bounds for all Λ^{+} and Λ^{-} when their product Λ is equal to $\frac{1}{4}$. Moreover, since the BGK model with $\tau = 1$ ($\Lambda^{\pm} = \frac{1}{2}$) belongs to the OTRT subclass, and, in turn, this BGK configuration is equivalent to the forward-time finite-difference schemes [24] (FTCS/MFTCS), the OTRT schemes may become more efficient (in terms of the number of the time steps) than the FTCS/MFTCS, either when $\Lambda^{-} > \frac{1}{2}$ for diffusion-dominant problems, or when $\Lambda^{-} < \frac{1}{2}$ for advection-dominant problems. The developments [23] make available: (i) the principal necessary stability conditions for the TRT AADE schemes; (ii) the proof of their *sufficiency* for the OTRT minimal models, such as the d1Q3, d2Q5 and d3Q7, with or without numerical diffusion; (iii) the generic OTRT sufficient conditions suitable for any AADE equilibrium; and (iv), the list of the most stable equilibrium weights for "full" OTRT schemes based on the d2Q9 and d3Q15 velocity sets.

The d1Q3 OTRT subclass is stable inside the whole triangle $U^2(c_e)$ in Fig. 1 for any Λ^{-}; the modeled diffusion coefficient is equal to $\Lambda^{-}c_e$, with free equilibrium parameter $c_e \in [0, 1]$. In contrast, the complex interplay of the exact d1Q3 stability curves $U^2(c_e, \Lambda^{-}, \Lambda)$ (they are built in this paper) takes place when Λ varies below $\Lambda = \frac{1}{4}$. The stable areas (below the curves) may become not only smaller than the optimal triangles but also smaller than the BGK stable subdomain. Also, the stability curves are not monotonic with respect to Λ and they may intersect the non-negativity line (*n-line*) even when Λ is very close to the optimal value $\Lambda = \frac{1}{4}$ (see the dotted line). The *n-line* guarantees the non-negativity of all equilibrium components. This condition is proved to be sufficient, *for any eigenvalue*, for stability of (i) the TRT pure diffusion operator and (ii) both the BGK and OTRT advection–diffusion models [23]. However, the non-negativity of all the individual equilibrium functions is not necessary for the stability of the OTRT subclass, but the evidence suggests that this condition is necessary in the BGK limit $\Lambda^{-} \to 0$. Hence, we want to prevent a blind use of Λ whose role may become equivocal: rewarding for

Please cite this article in press as: A. Kuzmin, et al., The role of the kinetic parameter in the stability of two-relaxation-time advection–diffusion lattice Boltzmann schemes, Computers and Mathematics with Applications (2010), doi:10.1016/j.camwa.2010.07.036

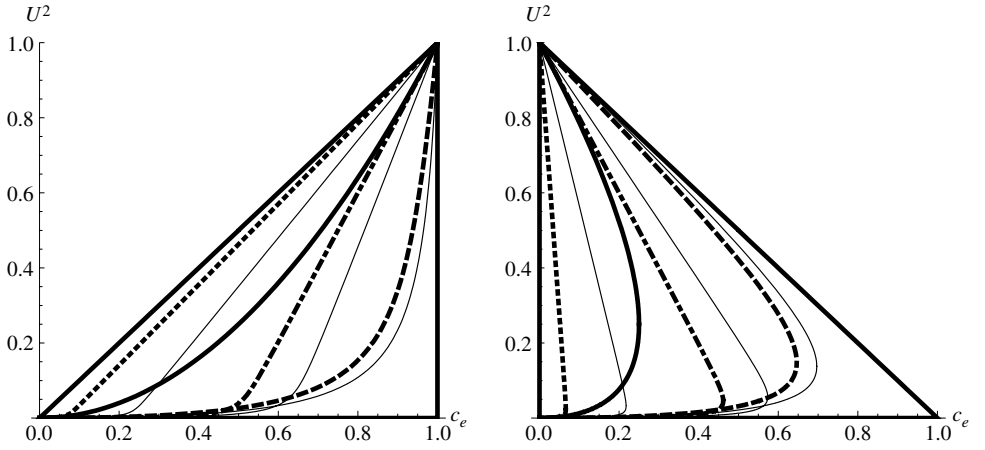

Fig. 1. When $\Lambda < \frac{1}{4}$, the stable domain lies under the stability curves $U^2(c_e, \Lambda_{bgk}, \Lambda)$ plotted here for $\Lambda^- = 10^{-2}$ ($\tau = 0.51$). The negative numerical diffusion $-\Lambda^- U^2$ has been corrected in the right picture. The BGK solution with $\Lambda = (\Lambda^-)^2$ very closely approaches **the thick solid curve** which is the non-negativity boundary. From the leftmost to the rightmost curve: $\Lambda = \{\Lambda^{(n,+)} \approx 0.23$ (dotted), $\frac{3}{16}$ (solid), $\Lambda^{(s,+)} \approx 0.12$ (dotted–dashed), $\frac{1}{12}$ (solid), $\Lambda^{(s,\max)} \approx 8 \times 10^{-3}$ (dashed), 10^{-6} (solid)$\}$. Here, only $\Lambda = 10^{-6}$ (the last curve) is smaller than the BGK value $(\Lambda^-)^2$. Further details are given in Table 4.

accuracy (with no extra efforts, e.g., decreasing Λ for high Λ^-) but penalizing the stability when $\Lambda \neq \frac{1}{4}$. We first examine how to select a pair $\{\Lambda^-, \Lambda\}$ where either the optimal curves (extended optimal subclass, EOTRT), the BGK curves, or else the non-negativity curves guarantee the stability for the d1Q3 model. Next we show that the d1Q3 stability curves on the one hand, and the necessary and sufficient conditions for its own OTRT subclass on the other hand, are necessary for any multi-dimensional model, and derive several conclusions.

The paper is organized as follows. Section 2 summarizes the principal results [23] for necessary (any TRT model) and sufficient (*a priori*, only the OTRT subclass) stability conditions. They are given in most detail for the isotropic minimal models and several selected d2Q9 and d3Q15 schemes, including their popular ("hydrodynamic") equilibrium form. Section 3 is focused on the construction and analysis of the d1Q3 stability curves $U^2(c_e, \Lambda^-, \Lambda)$. The BGK model is included for $(\Lambda^-)^2 = \Lambda$. Section 3.4 adapts the d1Q3 curves, along with the necessary conditions and non-negativity lines, as valuable guidelines for multi-dimensional models. Section 5 concludes this work. Tables 3 and 4 list the principal notation. Further technical details on the d1Q3 stability curves are provided in Appendix A. In Appendix B, we prove that the non-negativity conditions are necessary for the minimal BGK models in the advection limit, and then provide the non-negativity conditions for principal schemes. Appendix C contains the details of the numerical stability analysis.

2. The TRT AADE model

2.1. The evolution equation and necessary advection-dominant conditions

The TRT operator [6] possesses two relaxation parameters $\lambda^\pm \in]-2, 0]$:

$$f_q(\vec{r} + \vec{c}_q, t+1) = f_q + \lambda^+(f_q^+ - e_q^+) + \lambda^-(f_q^- - e_q^-), \tag{1}$$

where $f_q^\pm = \frac{f_q \pm f_{\bar{q}}}{2}$, $\vec{c}_q = -\vec{c}_{\bar{q}}$, $q = 0, \ldots, Q_m$.
In what follows, we operate with two positive eigenvalue functions Λ^- and Λ^+, and adapt two auxiliary symbols: (i) Λ for their product and (ii) Λ_{bgk} for Λ^{-2}:

$$\Lambda = \Lambda^-\Lambda^+, \quad \Lambda_{bgk} = \Lambda^{-2}, \quad \Lambda^\pm = -\left(\frac{1}{2} + \frac{1}{\lambda^\pm}\right), \quad -2 < \lambda^\pm < 0. \tag{2}$$

Historically, Λ is called the "magic" parameter. The BGK model fixes Λ by τ: $\lambda^+ = \lambda^- = -\frac{1}{\tau}$ and then $\Lambda = \Lambda_{bgk} = \frac{(2\tau-1)^2}{4}$; hereafter we mean $\tau = \frac{1}{2} + \sqrt{\Lambda_{bgk}}$. The equilibrium values $\{e_q^\pm = \frac{e_q \pm e_{\bar{q}}}{2}\}$ are prescribed for each pair of opposite lattice velocities $(q, \bar{q})$ assuming the mass constraint, $\sum_{q=0}^{Q_m} e_q^+ = \sum_{q=0}^{Q_m} f_q^+ = \sum_{q=0}^{Q_m} f_q = s$:

$$e_q = e_q^+ + e_q^- = sE_q, \quad E_q = E_q^+ + E_q^-, \quad q = 0, \ldots, Q_m,$$
$$e_q^+ = sE_q^+, \quad E_q^+ = E_q^{(m)} + g^{(u)}E_q^{(u)}(\vec{U}), \quad E_q^{(m)} = t_q^{(m)}c_e + E_q^{(anis)},$$

Please cite this article in press as: A. Kuzmin, et al., The role of the kinetic parameter in the stability of two-relaxation-time advection–diffusion lattice Boltzmann schemes, Computers and Mathematics with Applications (2010), doi:10.1016/j.camwa.2010.07.036

$$e_0^+ = e_0 = sE_0, \quad E_0 = 1 - \sum_{q=1}^{Q_m} E_q^+, \quad e_0^- = 0,$$

$$e_q^- = sE_q^-, \quad E_q^- = t_q^{(a)}(\vec{U}\cdot\vec{c}_q), \quad q = 1, \ldots, Q_m. \tag{3}$$

Here, the freely tunable parameter c_e is restricted to the interval $[0, c_e^{(\max)}]$ and prescribed by the necessary stability conditions of the pure diffusion equation (relations (17)–(20) when $\vec{U} \equiv 0$). The trace value of the *modeled diffusion tensor* $\Lambda^-\mathcal{D}$ is equal to $\Lambda^- c_e$ multiplied by the dimension d of the velocity set. A fully anisotropic tensor $\mathcal{D}$ can be obtained using the d2Q9 and d3Q15 models (where $\sum_{\alpha\neq\beta} c_{q\alpha}^2 c_{q\beta}^2 \neq 0$):

$$E_q^{(anis)} = \frac{1}{2}\sum_{\alpha=1}^{d}(\mathcal{D}_{\alpha\alpha} - c_e)c_{q\alpha}^2 + \frac{\sum_{\alpha\neq\beta}\mathcal{D}_{\alpha\beta}c_{q\alpha}c_{q\beta}}{\sum_{\alpha\neq\beta}c_{q\alpha}^2 c_{q\beta}^2}. \tag{4}$$

The (anisotropic) term $E_q^{(anis)}$ vanishes for isotropic tensors, $\mathcal{D}_{\alpha\beta} = c_e\delta_{\alpha\beta}$. The first term in relation (4) vanishes for the diagonal links where $\sum_\alpha c_{q\alpha}^2 = d$. The minimal models d2Q5 and d3Q7 are depleted of diagonal links and thus cannot describe the off-diagonal elements $\mathcal{D}_{\alpha\beta}$ with the local equilibrium corrections. More precisely, assuming that the mass ($t_q^{(m)}$) and advection ($t_q^{(a)}$) weights obey

$$\sum_{q=1}^{Q_m} t_q c_{q\alpha}c_{q\beta} = \delta_{\alpha\beta}, \quad \forall\,\{\alpha,\beta\} = 1, \ldots, d, \tag{5}$$

the TRT model results in the linear advection–diffusion equation

$$\partial_t s + \vec{U}\cdot\nabla s = \Lambda^- \sum_{\alpha,\beta}\mathcal{D}_{\alpha\beta}^{(eff)}\partial_{\alpha\beta}^2 s \tag{6}$$

with the *effective diffusion tensor* $\Lambda^-\mathcal{D}^{(eff)}$:

$$\mathcal{D}_{\alpha\beta}^{(eff)} = \mathcal{D}_{\alpha\beta}^+ - U_\alpha U_\beta, \quad \mathcal{D}_{\alpha\beta}^+ = \mathcal{D}_{\alpha\beta} + g^{(u)}\sum_{q=1}^{Q_m} E_q^{(u)} c_{q\alpha}c_{q\beta}, \quad g^{(u)} \in \{0, 1\},$$

$$\mathcal{D}_{\alpha\beta} = c_e\delta_{\alpha\beta} + \sum_{q=1}^{Q_m} E_q^{(anis)} c_{q\alpha}c_{q\beta}, \quad c_e = \frac{\sum_{\alpha=1}^{d}\mathcal{D}_{\alpha\alpha}}{d}. \tag{7}$$

When $g^{(u)} = 0$, the numerical diffusion is not eliminated and $\mathcal{D}_{\alpha\beta}^{(eff)} = \mathcal{D}_{\alpha\beta} - U_\alpha U_\beta$. When $g^{(u)} = 1$, the role of $E_q^{(u)}(\vec{U})$ is to remove the anisotropic tensor of the numerical diffusion $\{-U_\alpha U_\beta\}$ (see [6,22] for the derivation of this term). Using relation (4) and assuming that the weight family $\{t_q^{(u)}\}$ also obeys relation (5), the d2Q9 and d3Q15 models set

$$E_q^{(u)}(\vec{U}) = t_q^{(u)}\bar{U^2} + \frac{1}{2}\sum_{\alpha=1}^{d}(U_\alpha^2 - \bar{U^2})c_{q\alpha}^2 + \frac{g_{\alpha\beta}^{(u)}\sum_{\alpha\neq\beta}U_\alpha U_\beta c_{q\alpha}c_{q\beta}}{\sum_{\alpha\neq\beta}c_{q\alpha}^2 c_{q\beta}^2},$$

$$U^2 = \sum_\alpha U_\alpha^2, \quad \bar{U^2} = \frac{U^2}{d}. \tag{8}$$

When $g^{(u)} = 1$ but $g_{\alpha\beta}^{(u)} = 0$, only the diagonal elements $-U_\alpha^2$ are eliminated: $\mathcal{D}_{\alpha\alpha}^{(eff)} = \mathcal{D}_{\alpha\alpha}$, $\mathcal{D}_{\alpha\beta}^{(eff)} = \mathcal{D}_{\alpha\beta} - U_\alpha U_\beta$, $\alpha \neq \beta$. The positive semi-definiteness of the *effective* diffusion tensor gives necessary stability conditions. Hereafter, this is guaranteed by the *advection line*, or *a-line*. When $\mathcal{D}_{\alpha\beta}$ is isotropic, the *a-line* reads [23]

$$g^{(u)} = 0 : U^2 \le c_e, \quad d = \{1, 2, 3\}. \tag{9}$$

$$g^{(u)} = 1, \quad g_{\alpha\beta}^{(u)} = 0 : U^2 \le \frac{d}{d-1}c_e, \quad d = \{2, 3\}. \tag{10}$$

When $g^{(u)}g_{\alpha\beta}^{(u)} = 1$ in relation (8), the d2Q9 and d3Q15 models eliminate the full second-order tensor of their numerical diffusion, and then $\mathcal{D}^{(eff)} = \mathcal{D}$ and $\mathcal{D}^{(eff)}$ is positive semi-definite along with the prescribed diffusion tensor $\mathcal{D}$.

We restrict three (independent) families of weights: $\{t_q^{(m)}\}$, $\{t_q^{(a)}\}$, and $\{t_q^{(u)}\}$ to be non-negative and isotropic, i.e., they take the same value per class: say, $t_c^{(\cdot)}$ for all "coordinate" links and $t_d^{(\cdot)}$ for all "diagonal" links. All obey relation (5); hence

Please cite this article in press as: A. Kuzmin, et al., The role of the kinetic parameter in the stability of two-relaxation-time advection–diffusion lattice Boltzmann schemes, Computers and Mathematics with Applications (2010), doi:10.1016/j.camwa.2010.07.036

selecting $t_c^{(\cdot)}$ in the interval $[0, \frac{1}{2}]$, one obtains the non-negative weight $t_d^{(\cdot)} = \frac{1-2t_c^{(\cdot)}}{Q_m-2d}$. The d2Q5 and d3Q7 can be then viewed as the respective (coordinate) subclasses of the d2Q9 and d3Q15 schemes taking $t_c^{(m)} = t_c^{(a)} = t_c^{(u)} = \frac{1}{2}$, and then $t_d^{(\cdot)} = 0$:

$$\mathrm{dDQ}(2\mathrm{D}+1): E_q^{(m)} = \frac{\mathcal{D}_{\alpha\alpha}}{2}, \quad E_q^{(u)} = \frac{U_\alpha^2}{2} \quad \text{if } c_{q\alpha} \neq 0,\ q = 1, \ldots, Q_m. \tag{11}$$

This equilibrium is also suitable for the d1Q3 model where $\mathcal{D}_{\alpha\alpha} = c_e$. The minimal models are restricted to diagonal diffusion tensors $\mathcal{D}_{\alpha\alpha}$ in the presence of the off-diagonal numerical diffusion $-U_\alpha U_\beta, \alpha \neq \beta$. The immobile weight is independent of the anisotropy for all the models:

$$E_0(c_e, U^2) = 1 - c_e \sum_{q=1}^{Q_m} t_q^{(m)} - g^{(u)} U^2 \sum_{q=1}^{Q_m} t_q^{(u)}, \quad \text{then} \tag{12}$$

$$\mathrm{dDQ}(2\mathrm{D}+1): E_0(c_e, U^2) = 1 - dc_e - g^{(u)} U^2, \quad d = 1, 2, 3. \tag{13}$$

We refer to the function $U^2(c_e)$ such that $E_0(c_e, U^2) = 0$ and $U^2(c_e = c_e^{(0)}) = 0$ as the E_0-*non-negativity line* or the E_0-*n-line*. Then E_0 is non-negative if the local value U^2 is not higher than $U^2(c_e)$ when $c_e \in [0, c_e^{(0)}]$. When $g^{(u)} = 0$, the E_0-*n-line* reduces to (vertical) line $c_e = c_e^{(0)}$. We do not restrict $\{E_q\}$, $\{E_q^+\}$ or E_0 to be non-negative *a priori*. These constraints are discussed in two next sections.

2.2. The characteristic equation and necessary diffusion-dominant conditions

Prescribing Fourier modes: $f_q^\pm(\vec{r} + \vec{c}_q, t+1) = \Omega f_q^\pm(\vec{r}, t)\mathrm{e}^{\mathrm{i}k_q}$, as the solution of evolution equation in a periodic domain, the set $\{F_q^\pm(\vec{r}, t) = f_q^\pm / s(\vec{r}, t)\}$, $q = 0, \ldots, Q_m$, solves the following equations:

$$\Omega(F_q^+ + F_q^-)\mathrm{e}^{\mathrm{i}k_q} = (1+\lambda^+)F_q^+ + (1+\lambda^-)F_q^- - \lambda^+ E_q^+ - \lambda^- E_q^-. \tag{14}$$

Their solution as a function of Ω is

$$\begin{cases} F_0^+ = \dfrac{E_0\lambda^+}{1+\lambda^+-\Omega}, \\ F_q^+ = [(1-\Omega\cos[k_q]+\lambda^-)\lambda^+ E_q^+ + \mathrm{i}\Omega\sin[k_q]\lambda^- E_q^-]z_q, \\ F_q^- = [(1-\Omega\cos[k_q]+\lambda^+)\lambda^- E_q^- + \mathrm{i}\Omega\sin[k_q]\lambda^+ E_q^+]z_q, \\ z_q = [\Omega^2 - \Omega\cos[k_q](2+\lambda^++\lambda^-) + (1+\lambda^-)(1+\lambda^+)]^{-1}. \end{cases} \tag{15}$$

The Qth-order TRT characteristic equation for $\Omega = \{\Omega_q, q = 1, \ldots, Q_m\}$ is the mass conservation relation, $\sum_{q=0}^{Q_m} F_q^+ = 1$, or, equivalently,

$$F_0^+ + 2\sum_{q=1}^{Q_m/2} F_q^+ = 1. \tag{16}$$

The linear stability is guaranteed in the von Neumann sense (necessary and sufficient condition) when all $|\Omega_q| \leq 1$ for any $\vec{k}$. We look for the non-trivial necessary and sufficient stability conditions on the equilibrium weights $\{E_q^+\}$ and $\{E_q^-\}$ such that $|\Omega_q| \leq 1$ for any $\vec{k}$. Then we organize these conditions in the form of a stability curve $U^2(c_e)$. They give the minimum over all possible orientations of $\vec{U}$ and bound the stable subdomain in the plane (c_e, U^2), for *every pair of two eigenvalues and given equilibrium configuration*. When $\vec{k} \to 0$, the necessary stability conditions reduce to *a-lines* (9) and (10). Hereafter, the diffusion line, or *d-line*, is the segment of the stability curve which guarantees necessary stability conditions when $\vec{k}$ is either parallel to any one lattice axis: $\vec{k} = \pi\vec{1}_\alpha$, or parallel to their diagonal direction: $\vec{k} = \pi\vec{1}_d$. Then $\{E_q^-\}$ vanishes in the characteristic equation (along with $\sin[k_q]$) and the *necessary diffusion-dominant* conditions take the form [23]

$$\vec{k} = \pi\vec{1}_\alpha, \quad \mathrm{d2Q9, d3Q15}: 0 \leq \mathcal{D}_{\alpha\alpha}^+ \leq 1, \quad \mathcal{D}_{\alpha\alpha}^+ = \mathcal{D}_{\alpha\alpha} + g^{(u)}U_\alpha^2, \tag{17}$$

$$\vec{k} = \pi\vec{1}_d, \quad \mathrm{d2Q9}: 0 \leq E_0 + \sum_{q:c_{qx}c_{qy}\neq 0} E_q^+ \leq 1, \tag{18}$$

$$\vec{k} = \pi\vec{1}_d, \quad \mathrm{d3Q15}: 0 \leq E_0 \leq 1, \tag{19}$$

$$\vec{k} = \pi\vec{1}_d^{(\gamma)}, \quad \mathrm{d3Q15}: 0 \leq \sum_{q:c_{q\gamma}=0} E_q^+ \leq 1, \quad \forall\ \gamma = 1, \ldots, d. \tag{20}$$

These conditions are necessary for any relaxation parameter $\lambda^\pm$. The minimal models are included as the particular subclasses (see relations (11)–(13)). The first condition (17), necessary for any velocity set, restricts E_0 to $[0, 1]$ for the d1Q3 model and all $\mathcal{D}_{\alpha\alpha}^+$ to $[0, 1]$ for multi-dimensional models. Then $U_\alpha^2 \leq 1 - \max_\alpha \mathcal{D}_{\alpha\alpha} \leq 1 - c_e$ if $g^{(u)} = 1$. Together, these

Please cite this article in press as: A. Kuzmin, et al., The role of the kinetic parameter in the stability of two-relaxation-time advection–diffusion lattice Boltzmann schemes, Computers and Mathematics with Applications (2010), doi:10.1016/j.camwa.2010.07.036

conditions necessarily prescribe

$$\text{all models: } U^2 \le 1 - c_e \text{ if } g^{(u)} = 1, \text{ and } c_e \in [0,1] \text{ if } g^{(u)} = \{0,1\}. \tag{21}$$

The second and third conditions (18) and (19) are independent of the anisotropy: they restrict E_0 to $[0, 1]$ for the minimal models and the d3Q15 model, but not for the d2Q9 model, in general. The inequality (20) restricts, for the d3Q15 model, the sum of E_q^+ to the interval $[0, 1]$, for any two coordinate links in the 2D plane perpendicular to the γ-axis when $\vec{k}$ is parallel to the diagonal axis in this plane.

In general, the stability curve may depend on the equilibrium parameters, such as $\vec{U}$, c_e and weight values, and both eigenvalues λ^+ and λ^-. The eigenvalue dependency has several general exceptions [23]. The first exception is the pure diffusion equation ($\vec{U} \equiv 0$, $E_q^- \equiv 0$) where the non-negativity of all the symmetric equilibrium weights $\{E_q^+\}$ is the sufficient stability condition for any eigenvalue $\lambda^\pm \in]-2, 0[$. Hence, $c_e \in [0, c_e^{(0)}]$ is sufficient for the stability of the *isotropic* diffusion equation when all the weights $\{t_q^{(m)}\}$ are non-negative. The second exception is the BGK AADE model where the non-negativity of all the Q components E_q is the sufficient stability condition, $\forall \tau > \frac{1}{2}$. Note that $E_q \ge 0$ implies $E_q^+ \ge 0$. The (optimal) OTRT subclass presents the third interesting exception.

2.3. The OTRT subclass: necessary and sufficient stability conditions

In contrast with the BGK model case, the eigenvalue function Λ^+, and hence Λ, is free for the TRT models, in the sense that Λ^+ may take any positive value without altering the second-order equation (6). The OTRT subclass is defined for one specific value:

$$\text{OTRT}: \Lambda = \frac{1}{4}, \quad \text{or} \quad \frac{\lambda^+ + \lambda^-}{2} = -1. \tag{22}$$

Indeed, the choice $\Lambda = \frac{1}{4}$ is the only one which reduces the characteristic TRT equation (16) to a quadratic equation, for any velocity set. This enables the analytical study of the OTRT stability limits [23]. Remarkably, they do not depend on the separate values $\Lambda^\pm$ and are equivalent to the BGK scheme with $\tau = 1$: this is the only BGK scheme with $\Lambda_{bgk} = \Lambda = \frac{1}{4}$. Several of the important results are:

(1) The OTRT *necessary and sufficient* stability bounds are set by the condition

$$\mathcal{A}^2 + \mathcal{B}^2 \le 1, \quad \forall \vec{k}, \text{ where}$$
$$\mathcal{A} = E_0 + \sum_{q=1}^{Q_m} \cos[k_q] E_q^+, \quad \mathcal{B} = \sum_{q=1}^{Q_m} \sin[k_q] E_q^-, \quad \text{and} \quad k_q = \vec{k} \cdot \vec{c}_q. \tag{23}$$

(2) The OTRT subclass is stable (a sufficient condition) if the following set of inequalities are satisfied:

$$\sum_{q=1}^{Q_m} \frac{(E_q^-)^2}{E_q^+} \le 1, \quad E_0 \ge 0 \quad \text{and} \quad \{E_q^+ > 0, \forall q = 1, \ldots, Q_m\}. \tag{24}$$

This criterion is independent of $\vec{k}$.

(3) The non-negativity of all the weights: $E_0 \ge 0$ and $\{E_q > 0\}$ is also sufficient for the stability of the OTRT subclass but this condition is stronger than the set of inequalities (24).

(4) The inequalities (24) guarantee, for the minimal models, the sufficiency of the *a-lines* (9) and (10) when $E_0 \ge 0$. The resulting conditions are illustrated in Fig. 2. When the numerical diffusion is corrected, the stable velocity of the d1Q3 OTRT scheme reaches $U^2(c_e = 0) = 1$, or the CFL number is equal to 1, as in the well known Lax–Wendroff one-dimensional ADE scheme (right diagram in Fig. 2).

(5) The inequalities (24) also guarantee the sufficiency of the *a-lines* for the d2Q9 and d3Q15 models with the same weights, $t_q^{(m)} = t_q^{(a)} = t_q^{(u)}$, at least provided that $\{E_q^+ > 0\}$ and $E_0 \ge 0$.

Several specific d2Q9 and d3Q15 OTRT schemes are selected from [23] and gathered in Table 1. Their sufficient stability conditions are formulated in Table 2. They have been directly validated for solution (23). In all of these configurations, the (minimal) constraints (17)–(20) are sufficient for the decreasing diffusion-dominant boundary segment. The OTRT subclasses of the d2Q9$^{(opt)}$ schemes with $t_c^{(m)} \in [0, \frac{1}{4}]$ and d3Q15$^{(opt)}$ ($t_c^{(m)} = 0$) (these two "optimal" families set $t_c^{(a)} = \frac{1}{4}$) possess the best possible stability of the d1Q3 OTRT scheme, given by two large triangles in Fig. 2.

We emphasize that conditions (9) and (10) are *necessary for any eigenvalues*, and they are *sufficient, along with the necessary diffusion-dominant conditions,* for the minimal OTRT models and selected "full" OTRT schemes (see the first two columns in Table 2): no other choice of the eigenvalues may have better stability conditions for the same equilibrium configuration. The sufficient advection-dominant condition of the BGK model, the non-negativity of all "moving" equilibrium weights E_q, is much stronger than the *a-line* of the OTRT schemes, e.g., the condition $U^2 \le c_e$ is

Please cite this article in press as: A. Kuzmin, et al., The role of the kinetic parameter in the stability of two-relaxation-time advection–diffusion lattice Boltzmann schemes, Computers and Mathematics with Applications (2010), doi:10.1016/j.camwa.2010.07.036

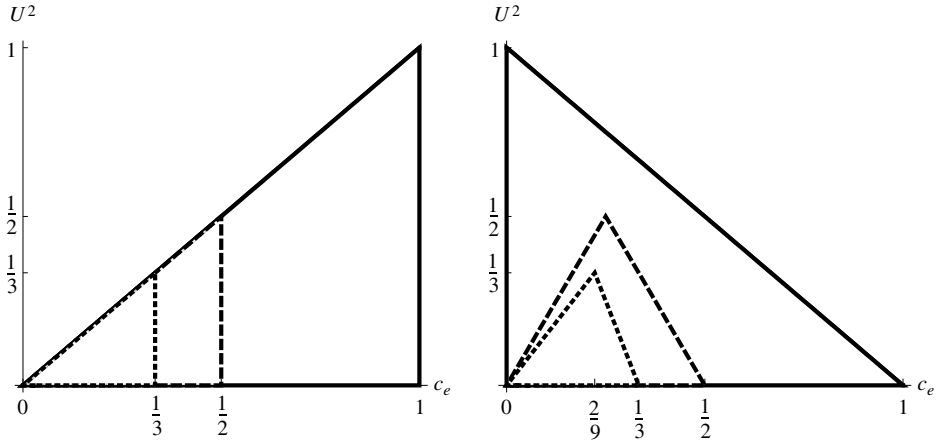

Fig. 2. The stable triangles are plotted for the minimal OTRT models: d1Q3 (large, solid boundary), d2Q5 (middle, dashed boundary) and d3Q7 (small, dotted boundary), for $g^{(u)} = 0$ (left, Eq. (9)) and $g^{(u)} = 1$ (right, Table 2). The increasing (left) edge is the *a-line* and decreasing (right) edge is the E_0*-n-line*. The diagram is recalled from [23].

Table 1
Equilibrium weights are specified for "standard", "uniform" and "optimal" models. The "standard" weights correspond to the "hydrodynamic" form: $E_q^{(u)} = \frac{t_q^{(m)}}{2}(3(\vec{U}\cdot\vec{c}_q)^2 - U^2)$, with $t_c^{(m)} = \frac{1}{3}$. The immobile weight $E_0(c_e, \vec{U} = 0)$ is non-negative when $c_e \in [0, c_e^{(0)}]$. The available stability interval for the OTRT subclass is $c_e \in [0, c_e^{(\max)}]$.

	$t_c^{(m)}$	$t_c^{(a)}$	$t_c^{(u)}$	$c_e^{(0)}$	$c_e^{(\max)}$
d2Q9$^{(stan)}$	$\frac{1}{3}$	$\frac{1}{3}$	$\frac{1}{6}$	$\frac{3}{5}$	$\frac{3}{4}$
d2Q9$^{(unif)}$	$\frac{1}{4}$	$\frac{1}{4}$	$\frac{1}{4}$	$\frac{2}{3}$	1
d2Q9$^{(opt)}$	$[0, \frac{1}{4}]$	$\frac{1}{4}$	$\frac{1}{2} - t_c^{(m)}$	$\frac{1}{1+2t_c^{(m)}}$	1
d3Q15$^{(stan)}$	$\frac{1}{3}$	$\frac{1}{3}$	0	$\frac{3}{7}$	$c_e^{(0)}$
d3Q15$^{(unif)}$	$\frac{1}{5}$	$\frac{1}{5}$	$\frac{1}{5}$	$\frac{5}{9}$	$c_e^{(0)}$
d3Q15$^{(opt)}$	$[0, \frac{1}{2}]$	$\frac{1}{4}$	$\frac{1}{2}$	$\frac{1}{1+4t_c^{(m)}}$	$c_e^{(0)}$

Table 2
The stability boundary $U^2(c_e)$ is given for the minimal and several "full" OTRT models when the modeled diffusion tensor $\mathcal{D}$ is isotropic. The highest velocity is reached when $c_e = c_e^{opt}$, which is the intersection of the increasing and decreasing segments of the stability curve.

	$g^{(u)} = 1, g_{\alpha\beta}^{(u)} = 0$		$g^{(u)} = 1, \{g_{\alpha\beta}^{(u)} = 1\}$	
	$U^2(c_e)$	c_e^{opt}	$U^2(c_e)$	c_e^{opt}
d1Q3	$1 - c_e$	0		
d2Q5	$\min\{2c_e, 1 - 2c_e\}$	$\frac{1}{4}$		
d3Q7	$\min\{\frac{3}{2}c_e, 1 - 3c_e\}$	$\frac{2}{9}$		
d2Q9$^{(stan)}$	$\min\{2c_e, 1 - c_e, 3 - 4c_e\}$	$\frac{1}{3}$	$\min\{\frac{3}{4}, 1 - c_e, 3 - 4c_e\}$	$[0, \frac{1}{4}]$
d2Q9$^{(unif)}$	$\min\{2c_e, 1 - c_e\}$	$\frac{1}{3}$	$1 - c_e$	0
d2Q9$^{(opt)}$	$\min\{2c_e, 1 - c_e\}$	$\frac{1}{3}$	$1 - c_e$	0
d3Q15$^{(stan)}$	$\min\{\frac{3}{2}c_e, 3 - 7c_e\}$	$\frac{6}{17}$	$\min\{2c_e, 3 - 7c_e\}$	$\frac{1}{3}$
d3Q15$^{(unif)}$	$\min\{\frac{3}{2}c_e, \frac{5}{3} - 3c_e\}$	$\frac{10}{27}$	$\min\{2c_e, \frac{5}{3} - 3c_e\}$	$\frac{1}{3}$
d3Q15$^{(opt)}$	$\min\{\frac{3}{2}c_e, 1 - \frac{c_e}{c_e^{(0)}}\}$	$\frac{2c_e^{(0)}}{3c_e^{(0)}+2}$	$1 - \frac{c_e}{c_e^{(0)}}$	0

to be contrasted with the non-negativity condition $U^2 \le c_e^2$ for the minimal models, and is yet stronger: $U^2 \le \frac{c_e^2}{d}$ for "full" models. The difference between the BGK and OTRT sufficient advection stability limits is crucial when the numerical diffusion is removed, especially when c_e is small (cf. conditions in Table 2 and the *n-lines* in Appendix B.2 for $g^{(u)} = 1$, plotted in Figs. 12–16). Hence, the OTRT subclass possesses much more advantageous sufficient advection stability criteria than the BGK model, especially in the limit $\Lambda_{bgk} \to 0$ where the non-negativity conditions become necessary for the BGK model.

The derivation of the stability conditions when $E_q^{(anis)} \neq 0$ (anisotropic tensors) is in progress. In this work, we restrict ourselves to the isotropic tensor $\mathcal{D}_{\alpha\beta} = c_e\delta_{\alpha\beta}$ ($\{E_q^{(anis)} = 0\}$) but extend the stability analysis beyond the OTRT subclass, starting from the d1Q3 model.

Please cite this article in press as: A. Kuzmin, et al., The role of the kinetic parameter in the stability of two-relaxation-time advection–diffusion lattice Boltzmann schemes, Computers and Mathematics with Applications (2010), doi:10.1016/j.camwa.2010.07.036

Table 3
List of principal notation.

Symbols	Meaning	Eqs./Figs.
Functions of two relaxation parameters $\lambda^{\pm} \in]-2, 0[$		
$\Lambda^{\pm} = -(\frac{1}{2} + \frac{1}{\lambda^{\pm}}) > 0$	Diffusion (Λ^-) and free (Λ^+) functions	(1), (2)
$\Lambda = \Lambda^+\Lambda^-$	Free "magic" parameter of the TRT model	(2)
$\Lambda_{bgk} = \Lambda^{-2} = (\tau - \frac{1}{2})^2$	Fixed Λ-value of the BGK model	(2)
$\Lambda = \frac{1}{4}$	Optimal TRT subclass (OTRT)	(22)
$\Lambda^{(ext.)}(\Lambda_{bgk}) \le \Lambda \le \frac{1}{4}$	Extended optimal TRT subclass (EOTRT)	(33)
Equilibrium parameters		
$E_q = E_q^+ + E_q^-, q = 1, \dots, Q_m$	The total weight of linear equilibrium $e_q = sE_q$	(3)
$E_0 = 1 - \sum_{q=1}^{Q_m} E_q^+$	The immobile weight	(3), (12)
$U^2 = \sum_{\alpha=1}^{d} U_\alpha^2, \bar{U}^2 = \frac{U^2}{d}$	Velocity amplitude (in square) and its mean value	(8)
$t_c^{(\cdot)} = \{t_c^{(m)}, t_c^{(a)}, t_c^{(u)}\} \in [0, \frac{1}{2}]$	Weights of the coordinate links	
$t_d^{(\cdot)} = \{t_d^{(m)}, t_d^{(a)}, t_d^{(u)}\} \in [0, \frac{1}{2}]$	Weights of the diagonal links	(5)
$E_q^- = t_q^{(a)}(\vec{U} \cdot \vec{c}_q)$	Provides advection term	(3), (6)
$E_q^+ = E_q^{(m)} + g^{(u)}E_q^{(u)}(\vec{U})$	Provides the d-rank tensor $\mathcal{D}^+$	(7)
$E_q^{(m)} = t_q^{(m)}c_e + E_q^{(anis)}, c_e \in [0, c_e^{(\max)}]$	Provides diffusion tensor $\mathcal{D}$ with the trace dc_e	(3), (7)
$E_q^{(anis)}$	Provides its anisotropic part: $\mathcal{D} - c_e\mathbb{1}$	(4)
$\Lambda^-\mathcal{D}^{(eff)} = \Lambda^-\{\mathcal{D}_{\alpha\beta}^+ - U_\alpha U_\beta\}$	Effective modelled diffusion tensor	(7)
$E_q^{(u)}$	Improves for the numerical diffusion $\{-U_\alpha U_\beta\}$	(8)
$g^{(u)} = 0$: $\mathcal{D}_{\alpha\beta}^+ = \mathcal{D}_{\alpha\beta}$	Numerical diffusion is presented in $\mathcal{D}^{(eff)}$	(8)
$g^{(u)}g_{\alpha\beta}^{(u)} = 1$: $\mathcal{D}_{\alpha\beta}^+ = \mathcal{D}_{\alpha\beta} + U_\alpha U_\beta$	Numerical diffusion is completely removed	(8)
$g^{(u)} = 1, g_{\alpha\beta}^{(u)} = 0$: $\mathcal{D}_{\alpha\beta}^+ = \mathcal{D}_{\alpha\beta} + U_\alpha U_\beta \delta_{\alpha\beta}$	Diagonal numerical diffusion $\{-U_\alpha^2\}$ is removed	(8)
Necessary stability conditions and non-negativity conditions for $U^2(c_e)$		
a-line	Guarantees $\det[\mathcal{D}^{(eff)}] \ge 0$	(9)–(10)
d-line is obtained when $\{k_\alpha\} \in \{0, \pi\}$	Guarantees diffusion-dominant conditions	(17)–(20)
E_0-*n-line*	Guarantees $E_0(c_e, U^2) \ge 0$ when $c_e \in [0, c_e^{(0)}]$	(12), (13)
n-line	Guarantees $E_q(\vec{U}) \ge 0$ for all $q = 1, \dots, Q_m$	(B.5)–(B.10)
$c_e^{(\max)}$	Highest c_e-value allowed by the *d-line*	Table 1
$c_e^{(0)} = \frac{1}{1+2(d-1)t_c^{(m)}}$	Highest c_e-value allowed by the E_0-*n-line*	Table 1
$c_e^{(p)}$ (peak)	Bisection of the *n-line* and the E_0-*n-line*	Fig. 13
$c_e^{(c)}$	Close to maximal curvature point	Figs. 13–16

3. The d1Q3 model

The equilibrium function of the d1Q3 model is given by relation (3) where E_q^+ is given by relation (11) with $\mathcal{D}_{\alpha\alpha} = c_e$ and $d = 1$, the immobile weight is made precise by relation (13). The necessary and sufficient "optimal" stability conditions of the OTRT subclass are set by *a-line* condition (9) in combination with the E_0-*n-line* (they bound two large triangles in Fig. 2):

$$g^{(u)} = 0 : 0 \le U^2 \le c_e, \quad 0 \le c_e \le 1,$$
$$g^{(u)} = 1 : 0 \le U^2 \le 1 - c_e, \quad 0 \le c_e \le 1. \tag{25}$$

These conditions are necessary for all velocity sets and any eigenvalues (cf. relations (17) and (21)). Then, for no one choice of the eigenvalues may the d1Q3 or any other model have better stability conditions than the d1Q3 OTRT subclass where these conditions are sufficient. In this section, we perform the analytical von Neumann stability analysis of the d1Q3 TRT model. We will show that the d1Q3 stability curves are *necessary* for any other velocity set.

3.1. Construction of stability curves

When $\vec{k}$ is parallel to one of the coordinate axis, $\vec{k} = k\vec{1}_\alpha$: (i) the components F_q^+ in relation (15) are equal to $\frac{E_q^+\lambda^+}{1+\lambda^+-\Omega}$ provided that the α-component of their velocity is zero ($c_{q\alpha} = 0$); (ii) all the others replace $\{\cos[k_q], \sin[k_q]\}$ with $\{\cos[k], \pm\sin[k]\}$ and obtain the same denominator z_q. Then the Qth-order characteristic equation (16) reduces to the *third-order equation for all considered velocity sets*:

$$P^{(3)}(\Omega) = 0, \quad \text{where}$$
$$\begin{aligned} P^{(3)}(\Omega) \;=\; & \Omega^3 - \Omega^2(1 + (1 - \cos[k])\lambda^+ s^+ + \cos[k](2 + \lambda^- + \lambda^+) + \mathrm{i}\lambda^- s^- \sin[k]) \\ & + \Omega((1 + \lambda^-)(1 + \lambda^+ - (1 - \cos[k])\lambda^+ s^+) + \cos[k](2 + \lambda^- + \lambda^+)) \\ & + \mathrm{i}\Omega(1 + \lambda^+)\lambda^- s^- \sin[k] - (1 + \lambda^+)(1 + \lambda^-), \quad \text{with } s^+ = \mathcal{D}_{\alpha\alpha}^+, s^- = U_\alpha, \text{ if } \vec{k} = k\vec{1}_\alpha. \end{aligned} \tag{26}$$

Please cite this article in press as: A. Kuzmin, et al., The role of the kinetic parameter in the stability of two-relaxation-time advection–diffusion lattice Boltzmann schemes, Computers and Mathematics with Applications (2010), doi:10.1016/j.camwa.2010.07.036

Table 4
Summary for the d1Q3 stability curves.

Symbols	Meaning	Eqs./Figs.
von Neumann analysis		
$\vec{k}$, $\{k_q = \vec{k}\cdot\vec{c}_q\}$	Wavevector and its projection on the velocity set	Eq. (14)
$\lvert\Omega(c_e, U^2, \Lambda_{bgk}, \Lambda, m)\rvert^2 = \frac{P_n(U^2)}{P_d(U^2)}$, where $m = \tan^2(\frac{k}{2})$ when $\vec{k} = k$	Root (in square) responsible for the stability of the d1Q3 model when $g^{(u)} = 0$	Eq. (A.1)
Stability curves: TRT and BGK d1Q3		
$\Lambda = \Lambda^{(ext.)}(\Lambda_{bgk})$	Boundary of the extended optimal subclass	Eq. (22)
$\Lambda \geq \Lambda^{(ext.)}(\Lambda_{bgk}), \forall \Lambda_{bgk}$	The TRT has the optimal stability	Eqs. (30), (31)
$\Lambda_{bgk} \geq \frac{1}{6}$	The BGK has the optimal stability	Eq. (30)
$U_0^{'}(\Lambda_{bgk}, \Lambda)$, $U_1^{'}(\Lambda_{bgk}, \Lambda)$	The slopes of stability curve at $U^2 = \{0, 1\}$	(A.13)–(A.14)
$\Lambda_{bgk}^{(crit.)} \approx 10^{-2}$ ($\tau^{(crit.)} \approx 0.6$)	$U_1^{'}(\Lambda_{bgk}, \Lambda) = U_1^{'}(\Lambda_{bgk}, \Lambda_{bgk})$ for $\Lambda > \Lambda_{bgk}$, exists when $\Lambda_{bgk} \leq 9.8 \times 10^{-3} < \Lambda_{bgk}^{(crit.)}$	
$\Lambda > \Lambda_{bgk}$ when $\Lambda_{bgk} < \Lambda_{bgk}^{(crit.)}$	The TRT may perform less well than the BGK for some c_e-interval	
"reliable" and "unreliable" families	$\Lambda_{bgk} \geq \Lambda_{bgk}^{(crit.)}$ and $\Lambda_{bgk} < \Lambda_{bgk}^{(crit.)}$, respectively	
$\Lambda > \Lambda_{bgk} > \Lambda_{bgk}^{(crit.)}$, $\Lambda_{bgk} < \frac{1}{6}$	The TRT is more stable than the BGK	
$\Lambda < \Lambda_{bgk} < \frac{1}{6}$	The BGK is more stable than the TRT	
Stability curves and non-negativity line (*n-line*)		
$\Lambda = \Lambda^{(s,\max)}(\Lambda_{bgk}) > \Lambda_{bgk}$ large unstable area	$U_1^{'}(\Lambda_{bgk}, \Lambda)$ has a local maximum on Λ, solution exists when $\Lambda_{bgk} \leq 8.4 \times 10^{-3}$	Figs. 1 and 7
$c_e = c_e^{(n)}$	Tangency point of the stability curve and *n-line*	Eq. (37), Fig. 8
$\Lambda^{(n,\pm)}(\Lambda_{bgk}) > \Lambda_{bgk}$	Stability curve touches the *n-line*, exists when $\Lambda_{bgk} \leq \Lambda_{bgk}^{(n)} \approx 7.36 \times 10^{-3}$	Eq. (38), Fig. 9(left)
$\Lambda \in]\Lambda^{(n,-)}, \Lambda^{(n,+)}[$, $\Lambda_{bgk} \leq \Lambda_{bgk}^{(n)}$	The stability is not guaranteed by the *n-line*	Fig. 8(right)
$\Lambda^{(s,\pm)}(\Lambda_{bgk}) > \Lambda_{bgk}$	$U_1^{'}(\Lambda_{bgk}, \Lambda^{(s,\pm)})$ is equal to *n-line*'s slope solution exists when $\Lambda_{bgk} \leq 6.37 \times 10^{-3}$	Eq. (39), Fig. 9(left)
$\Lambda^{(s)}(\Lambda_{bgk}) < \Lambda_{bgk}$, exists $\forall\ \Lambda_{bgk}$	$U_1^{'}(\Lambda_{bgk}, \Lambda^{(s)})$ is equal to *n-line*'s slope	
$\Lambda > \Lambda^{(s)}(\Lambda_{bgk})$ when $\Lambda_{bgk} \geq \Lambda_{bgk}^{(n)}$	The stability is guaranteed by the *n-line*	Figs. 5 and 6
$\Lambda < \Lambda^{(s)}(\Lambda_{bgk}), \forall\ \Lambda_{bgk}$	The stability is not guaranteed by the *n-line*	Fig. 9(right)

The equilibrium components appear only in two combinations: $s^+ = \sum_{q:c_{q\alpha}\neq 0} E_q^+ = \sum_{q=1}^{Q_m} E_q^+ c_{q\alpha}^2 = \mathcal{D}_{\alpha\alpha}^+$ and $s^- = \sum_{q=1:c_{q\alpha}\neq 0}^{Q_m/2}(E_q^- - E_{\bar{q}}^-) = U_\alpha$. As one particular case, Eq. (26) presents the d1Q3 characteristic equation for $\mathcal{D}_{\alpha\alpha}^+ = c_e + g^{(u)}U^2$ and $U_\alpha = U$. It follows that *the* d1Q3 *stability relations will become necessary for all the models.* They may become sufficient for the isotropic models provided that the worst situation happens when both $\vec{k}$ and $\vec{U}$ are parallel to the coordinate axis.

We look to establish stability curves $U^2(c_e)$ such that the three (complex) roots Ω have their amplitude $|\Omega|$ inside the interval [0, 1] when $|\vec{U}|^2 \leq U^2(c_e)$, for any direction of velocity vector $\vec{U}$ and any wavevector $\vec{k}$. The direct analysis of $|\Omega|$ seems to present a real challenge. Instead, we propose to apply twice Miller's Theorem 6.1 (see [25], p.403) which allows the sequential reduction of the nth-order polynomial equation $P^{(n)}(\Omega) = 0$ to the linear equation $P^{(1)}(\Omega) = 0$ with the equivalent von Neumann stability properties:

$$P^{(n-1)}(\Omega) = \frac{\tilde{P}^{(n)}(0)P^{(n)}(\Omega) - \tilde{P}^{(n)}(\Omega)P^{(n)}(0)}{\Omega}, \quad \text{if}$$

$$P^{(n)}(\Omega) = \sum_{j=0}^{n} a_j \Omega^j, \quad \tilde{P}^{(n)}(\Omega) = \sum_{j=0}^{n} a_{n-j}^* \Omega^j, \tag{27}$$

where $a^*{}_j$ is the complex conjugate of a_j. Miller's Theorem 6.1 states that if $|\tilde{P}^{(n)}(0)| > |P^{(n)}(0)|$ then $P^{(n)}(\Omega)$ is a von Neumann polynomial (i.e. the amplitude of all its roots is less than 1) when $P^{(n-1)}(\Omega)$ is a von Neumann polynomial. In fact, the pre-condition of Miller's Theorem, $|\tilde{P}^{(n)}(0)| > |P^{(n)}(0)|$, is satisfied owing to the eigenvalue stability conditions, $\lambda^\pm \in]-2, 0[$, provided that $c_e \in [0, 1]$.

Let Ω be the root of the von Neumann equivalent (27), the linear equation $P^{(1)}(\Omega) = 0$. It is suitable to present $|\Omega|^2$ as a ratio of two second-order polynomials, $P_n(U^2)$ and $P_d(U^2)$:

$$|\Omega|^2 = \frac{P_n(U^2)}{P_d(U^2)}, \quad \text{where}$$

$$P_n(U^2) = a_n + b_n U^2 + c_n U^4, \quad P_d(U^2) = a_d + b_d U^2 + c_d U^4. \tag{28}$$

The coefficients (28) are specified by relations (A.1) assuming the d1Q3 model with $g^{(u)} = 0$. They depend on Λ_{bgk}, Λ, c_e and k: hereafter we often use the auxiliary variable $m = \tan^2(\frac{k}{2})$, applying the transformation $\cos k \to \frac{1-m}{1+m}$, $\sin k \to \frac{2\sqrt{m}}{1+m}$

Please cite this article in press as: A. Kuzmin, et al., The role of the kinetic parameter in the stability of two-relaxation-time advection–diffusion lattice Boltzmann schemes, Computers and Mathematics with Applications (2010), doi:10.1016/j.camwa.2010.07.036

to Eq. (26). The solution (28) with (A.1) is suitable for other velocity sets with $\vec{k} = k\vec{1}_\alpha$ replacing c_e by $\mathcal{D}^+_{\alpha\alpha}$ and U by U_α. The necessary stability curves $U^2(c_e, \Lambda_{bgk}, \Lambda, m)$ solve equation $|\Omega|^2 = 1$, or, equivalently, $P_n(U^2) = P_d(U^2)$. When $g^{(u)} = 0$, this equation is quadratic with respect to the (non-negative) variable U^2. The *sufficient stability curve* $U^2(c_e, \Lambda_{bgk}, \Lambda)$ is the minimum of all the necessary curves over m:

$$g^{(u)} = 0 : U^2(c_e) = U_0^2(c_e, \Lambda_{bgk}, \Lambda), \quad \text{where}$$
$$U_0^2(c_e, \Lambda_{bgk}, \Lambda) = \min_{m>0}\{U^2(c_e, \Lambda_{bgk}, \Lambda, m) > 0 : P_n(U^2) = P_d(U^2)\}. \tag{29}$$

Hereafter, for the sake of simplicity, we often drop the dependency on Λ_{bgk} and Λ for stability curves $U^2(c_e)$. The interesting point is $c_e = 1$; then the solution (29) gives $U^2 = 1$ for any eigenvalues provided that $g^{(u)} = 0$. This agrees with the results of [19] for the d1Q2 BGK model (d1Q2 can be regarded as the limit of the d1Q3 for $c_e \equiv 1$). However, when the numerical diffusion is cancelled, the necessary condition $E_0 \geq 0$ prescribes $U^2(c_e = 1) = 0$.

3.2. The extended optimal subclass

The stability conditions (25) can be obtained by substituting $\Lambda = \frac{1}{4}$ into the original characteristic equation (16): this choice reduces its order to 2 and stability bounds are set by relations (23). Their necessity is predicted by relations (9) and (21) while the sufficiency can also be obtained with the OTRT criteria (24). With relations (A.4)–(A.5) one derives them directly from solution (28). Then the fourth-order expansion (A.6) of relation (28) in the limit $k \to 0$ shows that Λ_{bgk} and Λ should necessarily satisfy one of the two following conditions in order to prolong the "optimal" relations (25) for $\Lambda \neq \frac{1}{4}$:

$$\Lambda_{bgk} \geq \Lambda\frac{1-4\Lambda}{8\Lambda-1}, \quad \text{if } \frac{1}{8} < \Lambda \leq \frac{1}{4}, \text{ or } \Lambda \geq \frac{1}{4}, \ \forall\ \Lambda_{bgk}. \tag{30}$$

Both conditions are satisfied provided that

$$\Lambda \geq \Lambda^{(ext.)}(\Lambda_{bgk}), \quad \Lambda^{(ext.)} = \frac{1}{8}(1-8\Lambda_{bgk}) + \frac{1}{8}\sqrt{64\Lambda_{bgk}^2+1}, \quad \text{then} \tag{31}$$

$$\Lambda^{(ext.)}(\Lambda_{bgk}) \to \frac{1}{8}, \quad \text{if } \Lambda_{bgk} \to \infty,$$
$$\Lambda^{(ext.)}(\Lambda_{bgk}) \to \frac{1}{4}, \quad \text{if } \Lambda_{bgk} \to 0. \tag{32}$$

The EOTRT subclass is limited to $\Lambda = \frac{1}{4}$:

$$\text{EOTRT} : \Lambda^{(ext.)}(\Lambda_{bgk}) \leq \Lambda \leq \frac{1}{4}. \tag{33}$$

The EOTRT boundary (31) is illustrated in Fig. 3. The BGK model satisfies both conditions of (30) if $\Lambda_{bgk} = \Lambda \geq \frac{1}{6}$. When the two eigenvalues are related by condition (33), or when $\Lambda \geq \frac{1}{4}$, then $\max|\Omega|^2 \leq 1$ on the stability boundary (25). We also verified this result with the help of a numerical stability analysis. It follows that the d1Q3 TRT model retains the necessary and sufficient stability conditions (25) when $\Lambda \geq \Lambda^{(ext.)}(\Lambda_{bgk})$ for any Λ_{bgk}. The decreasing of Λ towards $\Lambda = \frac{1}{8}$ for high diffusion eigenvalue functions Λ_{bgk} is expected to improve their accuracy. However, $\Lambda^{(ext.)}(\Lambda_{bgk})$ very rapidly approaches $\Lambda = \frac{1}{4}$ for small diffusion functions, $\Lambda_{bgk} <\approx 10^{-2}$, where the EOTRT approaches the OTRT.

3.3. Beyond the extended optimal subclass, when $\Lambda \leq \Lambda^{(ext.)}$

When $\Lambda \leq \Lambda^{(ext.)}$, the solution $U_0^2(c_e, \Lambda_{bgk}, \Lambda)$ is given by a suitable non-negative root of the third-order equation:

$$a_0 + a_1 x + a_2 x^2 + a_3 x^3 = 0, \quad a_i(c_e, \Lambda_{bgk}, \Lambda) = \sum_{j=0}^{5} a_{i,j}(\Lambda_{bgk}, \Lambda)c_e^j. \tag{34}$$

The coefficients $\{a_{i,j}(\Lambda_{bgk}, \Lambda)\}$ of (fifth-order) polynomials are given by relations (A.8) for the BGK model and by relations (A.11)–(A.12) for the TRT model. The stability curve $U^2(c_e, \Lambda_{bgk}, \Lambda)$ for $g^{(u)} = 1$ can be constructed replacing c_e with $c_e + U^2$ in the solution obtained, $U_0^2(c_e)$, then solving the (fifth-order) equation with respect to U^2:

$$g^{(u)} = 1 : U^2 = U_0^2(c_e + U^2). \tag{35}$$

Two suitable (non-negative) roots which intersect the vertical axis in two limit points $U^2(0) = 0$ and $U^2(0) = 1$ are, respectively, the lower and upper segments of stability curve, up to their intersection. The d1Q3 stability curves are constructed with the help of routines [26] for the (analytical) solving of the minimization problem (29) and the (numerical) solving of the polynomial equations (35). We study them in the next two sections starting from the BGK subclass.

Please cite this article in press as: A. Kuzmin, et al., The role of the kinetic parameter in the stability of two-relaxation-time advection–diffusion lattice Boltzmann schemes, Computers and Mathematics with Applications (2010), doi:10.1016/j.camwa.2010.07.036

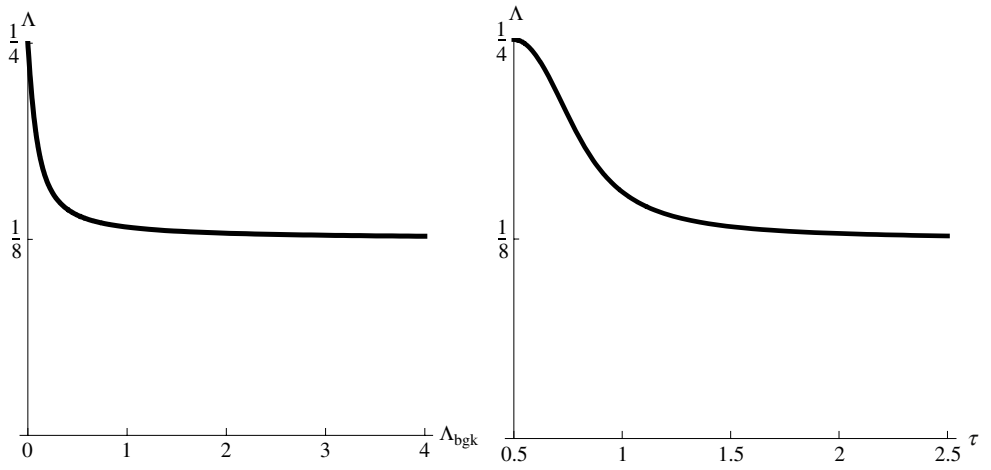

Fig. 3. The boundary $\Lambda = \Lambda^{(ext.)}$ of the extended optimal subclass EOTRT is plotted versus Λ_{bgk} (left) and versus τ, $\tau = \frac{1}{2} + \sqrt{\Lambda_{bgk}}$ (right).

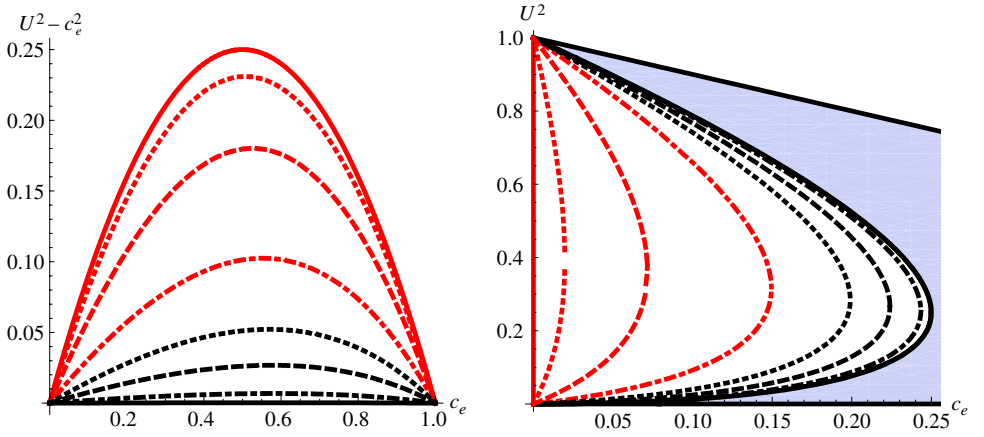

Fig. 4. The exact results for the d1Q3 BGK model show: (left picture) $U^2 - c_e^2$ when $g^{(u)} = 0$; (right picture) the stability curve $U^2(c_e)$ when $g^{(u)} = 1$—the stable area is limited by the $U^2(c_e)$ and the E_0-*n-line* $U^2 \le 1 - c_e$ when $c_e \in [0, 1]$. The BGK has the optimal stability conditions (25) when $\Lambda_{bgk} \ge \frac{1}{6}$. From the most stable to the least stable curve: $\Lambda_{bgk} = \Lambda = \{\frac{1}{6}$ (solid), $\frac{1}{8}$ (dotted), $\frac{1}{12}$ (dashed), $\frac{1}{24}$ (dotted–dashed), $\frac{1}{50}$ (thick dotted), $\frac{1}{100}$ (thick dashed), $\frac{1}{400}$ (thick dotted–dashed), 10^{-4} (thick solid)$\}$. The BGK curves are enveloped by the *n-line*, the maximum value $U^2 - c_e^2$ is less than 3×10^{-4} when $\Lambda_{bgk} = 10^{-4}$ (the "horizontal" solid line in the left picture).

3.3.1. *The BGK subclass*

The BGK subclass retains the optimal stability conditions (25) for any $\Lambda_{bgk} \ge \frac{1}{6}$. The necessity of the non-negativity condition in the limit $\Lambda = \Lambda_{bgk} \to 0$ is demonstrated in Appendix B.1 for the minimal models, as the limit of the exact BGK stability curve when $\vec{k} \parallel \vec{U}$. The sufficiency of this condition is proved for the BGK model with generic equilibrium (3) and any τ [23]. The following relations describe the domains where all equilibrium weights $\{E_q\}$ are non-negative, along with E_0, for the d1Q3 model:

$$g^{(u)} = 0 : 0 \le U^2 \le c_e^2, \quad 0 \le c_e \le 1,$$
$$g^{(u)} = 1 : c_e - U + U^2 \ge 0, \quad U > 0 \text{ and } U^2 \le 1 - c_e, \ 0 \le c_e \le 1. \tag{36}$$

The stability curves $U^2(c_e) = U_0^2(c_e, \Lambda_{bgk})$ are plotted in Fig. 4 for several Λ_{bgk} values, $\Lambda_{bgk} \le \frac{1}{6}$. Here, we plot the difference between the stability curve and the non-negativity line, $U^2(c_e) - c_e^2$, for $g^{(u)} = 0$ (left diagram) and $U^2(c_e)$ for $g^{(u)} = 1$ (right diagram). The solution $U^2(c_e)$ for $g^{(u)} = 0$ is described by a suitable root of the third-order equation (34) with the coefficients (A.8). The procedure (35) is applied to this solution when $g^{(u)} = 1$. The stability behaviour of the d1Q3 BGK model is relatively simple: the stable subdomain monotonically decreases when $\Lambda_{bgk} \to 0$, from the optimal domain (25) for $\Lambda_{bgk} \ge \frac{1}{6}$ towards the non-negativity domain (36).

Please cite this article in press as: A. Kuzmin, et al., The role of the kinetic parameter in the stability of two-relaxation-time advection–diffusion lattice Boltzmann schemes, Computers and Mathematics with Applications (2010), doi:10.1016/j.camwa.2010.07.036

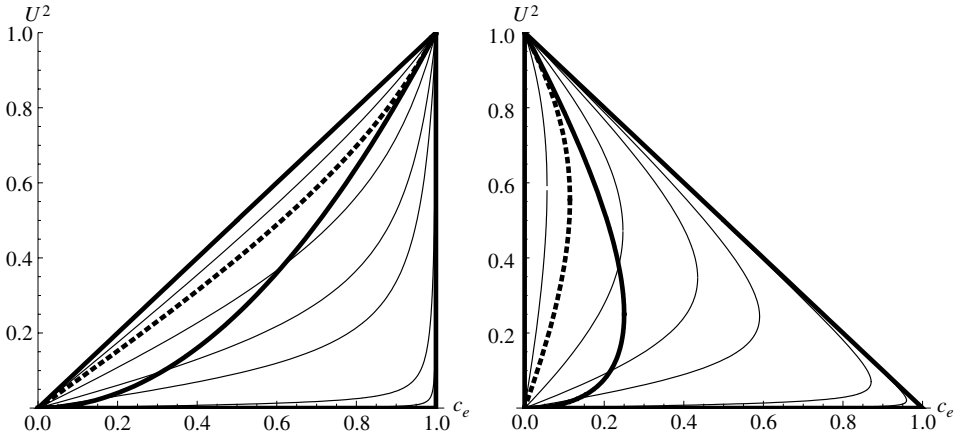

Fig. 5. Exact stability curves for the d1Q3 model with $g^{(u)} = 0$ (left) and $g^{(u)} = 1$ (right) are plotted for $\Lambda_{bgk} = 1$ ($\tau = \frac{3}{2}$) when $\Lambda = \{\frac{1}{12}, \Lambda^{(s)}$(dotted), $\frac{1}{25}, \frac{1}{50}, 10^{-2}, 10^{-3}, 10^{-4}\}$, from the most stable to least stable curve; the *n-line* is the thick solid line. The EOTRT subclass is stable for the whole triangle when $\Lambda \geq \Lambda^{(ext.)} \approx 0.133$. The stability curves first intersect the *n-line* when $\Lambda < \Lambda^{(s)} \approx 6.51 \times 10^{-2} < \Lambda_{bgk}$. When $\Lambda = 10^{-4}$, the stable area (almost) reduces to the segment $c_e = 1$ when $g^{(u)} = 0$ and it disappears for $g^{(u)} = 1$.

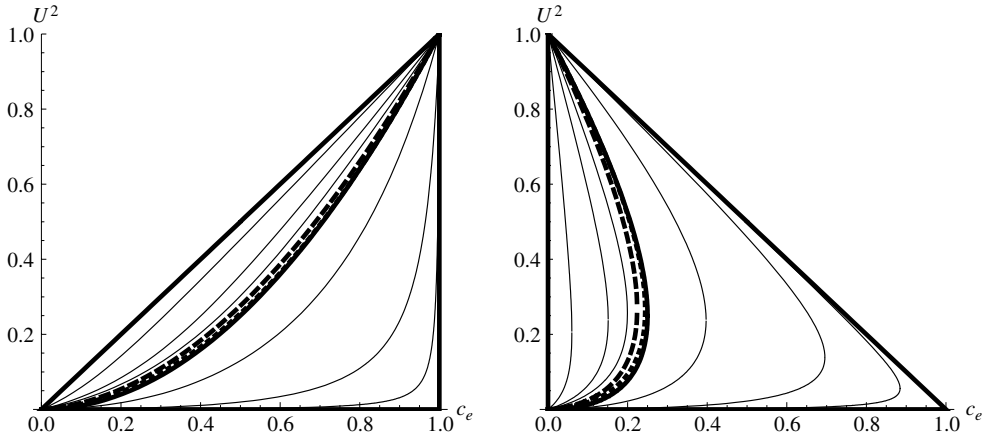

Fig. 6. Exact stability curves for the d1Q3 model with $g^{(u)} = 0$ (left) and $g^{(u)} = 1$ (right) are plotted for $\Lambda_{bgk} = 10^{-2} \geq \Lambda_{bgk}^{(crit.)}$ ($\tau = 0.6$) when, from the most stable to the least stable curve: $\Lambda = \{\frac{3}{16}, \frac{1}{8}, \frac{1}{12}, \Lambda_{bgk}$(dashed), $\Lambda^{(s)}$(dotted), $10^{-3}, 10^{-4}, 10^{-5}\}$; three first and three last lines are solid; the *n-line* is thick solid. The EOTRT subclass is stable for the whole triangle when $\Lambda \geq \Lambda^{(ext.)} \approx 0.24$ and the TRT is more stable than the BGK for $\Lambda > \Lambda_{bgk}$. The stability curves first cuts the *n-line* when $\Lambda < \Lambda^{(s)} \approx 5.47 \times 10^{-3} < \Lambda_{bgk}$.

3.4. The TRT model: "reliable" and "unreliable" families

We refer to the set of stability curves obtained for one (fixed) Λ_{bgk} value when Λ varies as the "family". Then every family includes its own BGK curve for $\Lambda = \Lambda_{bgk}$. Fig. 1 and Figs. 5–7 show the variety of stability curves for different families when Λ varies below $\Lambda = \frac{1}{4}$. Here, the two largest triangles are the OTRT conditions (25). The non-negativity line *n-line* (the thick solid line given by relation (36)) bounds the non-negativity domain. Four families are illustrated: "reliable" families with $\Lambda_{bgk} = 1$ in Fig. 5 and $\Lambda_{bgk} = 10^{-2}$ in Fig. 6, and "unreliable" families with $\Lambda_{bgk} = \frac{1}{400}$ in Fig. 7 and $\Lambda_{bgk} = 10^{-4}$ in Fig. 1. We keep in mind several particular values such as $\Lambda = \{\frac{3}{16}, \frac{1}{8}, \frac{1}{12}\}$, the BGK component of each family and the limit $\Lambda \to 0$. The figures show that all stable areas remain bounded by the E_0-*n-line* but the *a-line* drops such that the stable areas do not always monotonically decrease with Λ. Next, neither the BGK curve nor the *n-line* guarantees the stability for all eigenvalues and the stability curves are not controlled by Λ when $\Lambda < \frac{1}{4}$, in the sense that the same Λ may result in very different stable areas for different Λ_{bgk}.

What is the difference between "reliable" and "unreliable" families? One could expect that the TRT model will have better stability than its BGK subclass when $\Lambda > \Lambda_{bgk}$, and vice versa when $\Lambda < \Lambda_{bgk}$. The "reliable" families obey this rule but they cover only one part of Λ_{bgk}, namely $\Lambda_{bgk} \geq \Lambda_{bgk}^{(crit.)}$. In fact, the stability curves first intersect their BGK counterpart when $\Lambda_{bgk} \approx 9.8 \times 10^{-3}$; we then set $\Lambda_{bgk}^{(crit.)} \approx 10^{-2}$ (or $\tau^{crit.} \approx 0.6$). Hence, the TRT stability curves are enveloped by the BGK curves when $\Lambda_{bgk} \in [\Lambda_{bgk}^{(crit.)}, \frac{1}{6}]$ and $\Lambda \geq \Lambda_{bgk}$.

Please cite this article in press as: A. Kuzmin, et al., The role of the kinetic parameter in the stability of two-relaxation-time advection–diffusion lattice Boltzmann schemes, Computers and Mathematics with Applications (2010), doi:10.1016/j.camwa.2010.07.036

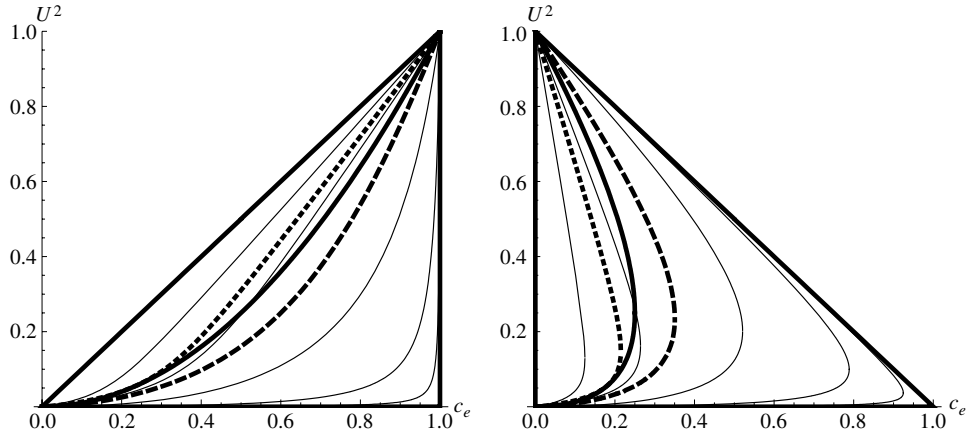

Fig. 7. Exact stability curves for the d1Q3 model with $g^{(u)} = 0$ (left) and $g^{(u)} = 1$ (right) are plotted in the "unreliable" zone $\Lambda_{bgk} < \Lambda_{bgk}^{(crit.)}$, where $\Lambda_{bgk} = \frac{1}{400}$ ($\tau = 0.55$) when, from the leftmost to the rightmost curve: $\Lambda = \{\frac{3}{16}$(solid), $\Lambda^{(n,+)}$(dotted), $\frac{1}{8}$(solid), Λ_{bgk}(thick solid), $\Lambda^{(s,\max)}$(dashed), 10^{-4}, 10^{-5}, $10^{-6}\}$. Data: $\Lambda^{(ext.)} \approx 0.246$, $\Lambda = \Lambda^{(s,\max)} \approx 2.78 \times 10^{-2}$, $\Lambda^{(s)} \approx 1.78 \times 10^{-3}$, $[\Lambda^{(n,-)}, \Lambda^{(n,+)}] \approx [4.21 \times 10^{-3}, 0.148]$ and $[\Lambda^{(s,-)}, \Lambda^{(s,+)}] = [4.24 \times 10^{-3}, 0.083]$. The largest unstable area for $\Lambda > \Lambda_{bgk}$ roughly corresponds to $\Lambda^{(s,\max)}$. Towards the BGK, the stable area increases but then drops again when $\Lambda \to 0$ (see the last three solid curves).

Next, the stability curve touches the non-negativity line at the (tangency) point $c_e = c_e^{(n)}$ when Λ_{bgk} and Λ are related as

$$c_e^{(n)} = 1 - 2\sqrt{\Lambda} \quad \text{if } \Lambda_{bgk}(\Lambda) = \frac{(1-2\sqrt{\Lambda})^2}{(1+2\sqrt{\Lambda})^2}\Lambda, \quad 0 < \Lambda < \frac{1}{4}. \tag{37}$$

The inverse solution has two roots:

$$\Lambda^{(n,\pm)}(\Lambda_{bgk}) = \frac{1 - 8\Lambda^- + 4\Lambda_{bgk} \pm (1-2\Lambda^-)\sqrt{1 - 12\Lambda^- + 4\Lambda_{bgk}}}{8},$$
$$\text{if } 0 < \Lambda_{bgk} \le \Lambda_{bgk}^{(n)} = \frac{1}{4(17+12\sqrt{2})} \approx 7.36 \times 10^{-3}, \quad \Lambda^- = \sqrt{\Lambda_{bgk}}. \tag{38}$$

When $\Lambda_{bgk} < \Lambda_{bgk}^{(n)}$, the stability curve intersects the non-negativity line when Λ belongs to the interval $]\Lambda^{(n,-)}, \Lambda^{(n,+)}[$ and touches it for $\Lambda = \Lambda^{(n,\pm)}(\Lambda_{bgk})$, with $\Lambda^{(n,+)} = \Lambda^{(n,-)} = \frac{3}{4} - \frac{\sqrt{2}}{2}$ when $\Lambda_{bgk} = \Lambda_{bgk}^{(n)}$. Hence, the behaviour of the stability curves is not monotonic with Λ in this interval and the non-negativity line does not guarantee the stability for the TRT curves on some part of the interval $c_e \in [0, 1]$. The variation of the $c_e^{(n)}$ with Λ_{bgk} is shown in the left picture in Fig. 8. The stability curves are shown in the right picture in Fig. 8 for three limit solutions: $\Lambda = \Lambda^{(n,\pm)}$ and $\Lambda = \Lambda^{(s)}$ (see below), along with the BGK solution $\Lambda = \Lambda_{bgk}$. The interval $[\Lambda^{(n,-)}, \Lambda^{(n,+)}]$ versus Λ_{bgk} is found between the lower and upper branches of the solid line in the left picture in Fig. 9: it lies above $\Lambda = \Lambda_{bgk}$. The exact boundary values of slopes of stability curves are given by relations (A.13) and (A.14). Inside the "unreliable" interval $\Lambda \in [\Lambda^{(n,-)}, \Lambda^{(n,+)}]$, the slope function $U_1'(\Lambda_{bgk}, \Lambda) = \frac{\partial U^2}{\partial c_e}(U^2 = 1)$ has the local maximum, say for $\Lambda = \Lambda^{(s,\max)}(\Lambda_{bgk})$. The largest unstable area when $\Lambda > \Lambda_{bgk}$ roughly corresponds to this value (see the dashed lines in Figs. 1 and 7).

Next, in a very narrow interval $\Lambda_{bgk} < \Lambda < \Lambda^{(n,-)}$, the stable area increases towards the BGK curve which lies above the non-negativity line, then decreases again. When $\Lambda = \Lambda^{(s)}(\Lambda_{bgk}) < \Lambda_{bgk}$, the slope of the stability curve and the slope of the non-negativity line become equal for $U^2 = 1$. The function $\Lambda = \Lambda^{(s)}(\Lambda_{bgk})$ solves Eq. (39) (with "+") and it is plotted in the right picture in Fig. 9:

$$\Lambda_{bgk}(\Lambda) = \Lambda\frac{1 + 16\Lambda - 64\Lambda^2 \pm 8\sqrt{(1-4\Lambda)\Lambda}}{(1-8\Lambda)^2}, \quad 0 < \Lambda < \frac{1}{8}. \tag{39}$$

Yet the stability curves for any $\Lambda_{bgk} > \Lambda_{bgk}^{(n)}$ lie above the non-negativity line (36) provided that $\Lambda \ge \Lambda^{(s)}(\Lambda_{bgk})$. This can be observed in Figs. 5 and 6 where the stability curves for $\Lambda = \Lambda^{(s)}(\Lambda_{bgk})$ are given by dotted lines. The values $\Lambda^{(s)}(\Lambda_{bgk})$ are smaller than Λ_{bgk} for any Λ_{bgk} and this function monotonically approaches the asymptotic line $\Lambda = \frac{1}{8}$ from below when $\Lambda_{bgk} \to \infty$, whereas the extended optimal boundary, $\Lambda = \Lambda^{(ext.)}(\Lambda_{bgk})$, asymptotically approaches the same line from above, in the same limit $\Lambda_{bgk} \to \infty$. Hence, the higher Λ_{bgk}, the smaller the interval $[\Lambda^{(s)}, \Lambda^{(ext.)}]$. Indeed, $U_1' \sim \frac{\Lambda_{bgk}}{4\Lambda}$ in the limit $\Lambda \to 0$ (the last relation of (A.14)); then U_1' is larger, and hence the stable domain is smaller, for high values Λ_{bgk} when Λ is very small (cf. the stability curves for $\Lambda_{bgk} = 1$ in Fig. 5 and the results for three other Λ_{bgk} values when

Please cite this article in press as: A. Kuzmin, et al., The role of the kinetic parameter in the stability of two-relaxation-time advection–diffusion lattice Boltzmann schemes, Computers and Mathematics with Applications (2010), doi:10.1016/j.camwa.2010.07.036

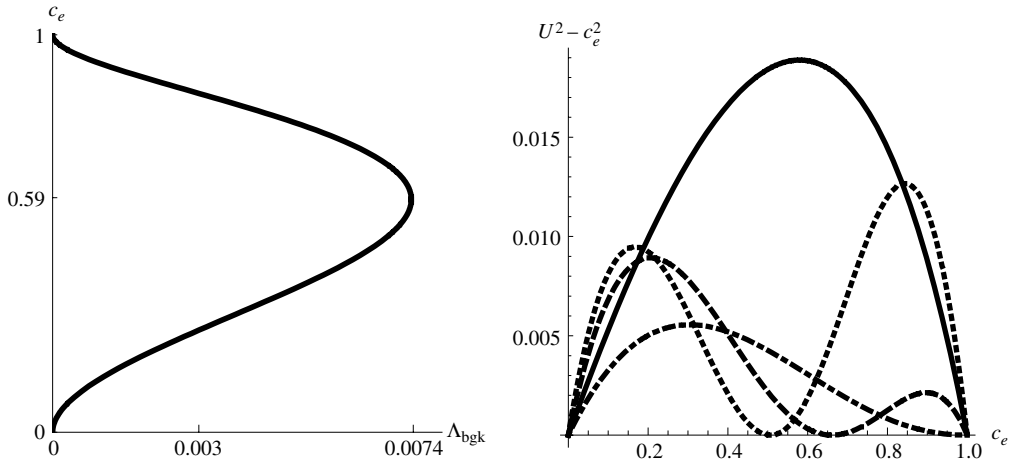

Fig. 8. The tangency point $c_e = c_e^{(n)}(\Lambda_{bgk})$ of the stability and non-negativity curves, given by relation (37), is plotted (left picture): $c_e^{(n)} \in [0, \sqrt{2}(\sqrt{2}-1)]$ when $\Lambda_{bgk} \in [0, \Lambda_{bgk}^{(n)}]$ and $\Lambda = \Lambda^{(n,+)}$; then $c_e^{(n)} \in [\sqrt{2}(\sqrt{2}-1), 1]$ when $\Lambda = \Lambda^{(n,-)} < \Lambda^{(n,+)}$. The difference between the stability curve and the *n-line* is illustrated (right picture) for $\Lambda_{bgk} = 7 \times 10^{-3} < \Lambda_{bgk}^{(n)}$ when $\Lambda = \Lambda_{bgk}$ (solid), $\Lambda = \Lambda^{(n,+)} \approx 6 \times 10^{-2}$ (dotted) and $\Lambda^{(n,-)} \approx 2.9 \times 10^{-2}$ (dashed). When $\Lambda < \Lambda^{(s)} \approx 4.2 \times 10^{-3} < \Lambda_{bgk}$ (dotted–dashed), the stability curve intersects the non-negativity line (Eq. (39)) for all Λ_{bgk}.

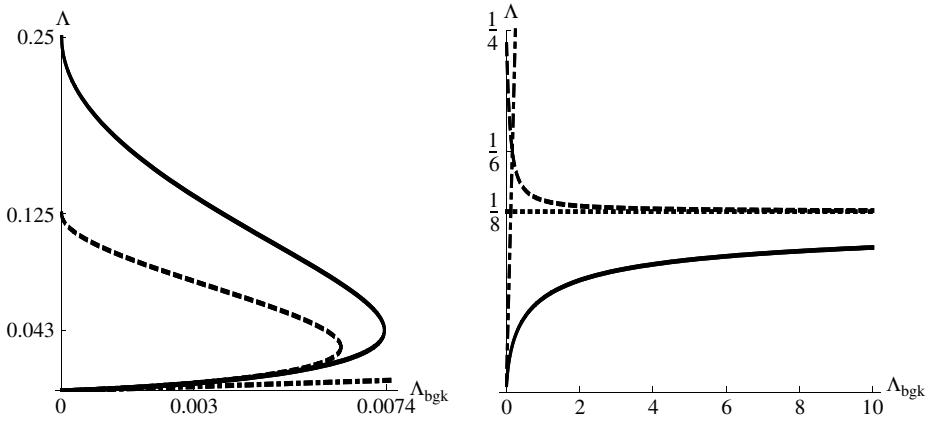

Fig. 9. Left picture: the functions $\Lambda = \Lambda^{(n,\pm)}(\Lambda_{bgk})$ (solid, Eq. (38)) and $\Lambda = \Lambda^{(s,\pm)}(\Lambda_{bgk})$ (dashed, Eq. (39) with "−"). All of them lie above $\Lambda = \Lambda_{bgk}$ (dotted–dashed) and they exist only if $\Lambda_{bgk} \le \Lambda_{bgk}^{(n)}$ and $\Lambda_{bgk} \le\approx 6.37 \times 10^{-3}$, respectively. Right picture: the function $\Lambda = \Lambda^{(s)}(\Lambda_{bgk}) < \Lambda_{bgk}$ (solid, Eq. (39) with "+") exists for any Λ_{bgk}; the dotted–dashed line is $\Lambda_{bgk} = \Lambda$; the dashed line is $\Lambda = \Lambda^{(ext.)}(\Lambda_{bgk})$.

$\Lambda \le 10^{-3}$). It follows that one should avoid a combination of very high Λ_{bgk} values with very small Λ, taking $\Lambda > \frac{1}{8}$ in the limit $\Lambda_{bgk} \to \infty$.

Finally, Fig. 10 verifies one "unreliable" situation, when $\Lambda_{bgk} = 10^{-4}$ (very small) and $\Lambda = \frac{1}{12}$ (relatively high and expected to be accurate). Typically, the stability curve is then decomposed into two segments: the first part is almost "horizontal", roughly up to the point of maximal curvature, $c_e \approx c_e^{(c)}(\Lambda_{bgk}, \Lambda)$; the second part is approximately linear, towards $U^2 = 1$. In fact, there is only a very small difference in stable velocity amplitude for $g^{(u)} = 0$ and $g^{(u)} = 1$ when $c_e \le c_e^{(c)} \approx \frac{U_1'-1}{U_1'}$. The $c_e^{(c)}$ is the same in both cases. When $\Lambda_{bgk} \to 0$ then $U_1'(\Lambda_{bgk}, \Lambda) \to \frac{1}{4\Lambda}$; hence $c_e^{(c)}$ is (asymptotically) equal to $1 - 4\Lambda$. We suggest avoiding the interval $c_e \in [0, \approx c_e^{(c)}(\Lambda_{bgk}, \Lambda)]$, especially when $\Lambda \in [\Lambda^{(n,-)}, \Lambda^{(n,+)}]$ and the stability is not controlled by the non-negativity line.

In summary, the d1Q3 model keeps the optimal stability (25) for any Λ_{bgk} when $\Lambda \ge \Lambda^{(ext.)}(\Lambda_{bgk})$. The BGK model shares this property when $\Lambda_{bgk} \ge \frac{1}{6}$. When $\Lambda \in]0, \Lambda^{(ext.)}(\Lambda_{bgk})[$, the exact stability curves are given by a suitable root of Eq. (34), along with relation (A.8) for the BGK model and relations (A.11)–(A.12) for the TRT model with any $\Lambda_{bgk} > 0$. The non-negativity conditions are given by relation (36); they guarantee stability of the BGK model. The TRT model has better stability than the BGK one for all $c_e \in [0, 1]$ when $\Lambda > \Lambda_{bgk} \ge \Lambda_{bgk}^{(crit.)}$, $\Lambda_{bgk}^{(crit.)} \approx 10^{-2}$. The TRT stability curve intersects the non-negativity line only for $\Lambda < \Lambda^{(s)}(\Lambda_{bgk}) < \Lambda_{bgk}$ provided that $\Lambda_{bgk} > \Lambda_{bgk}^{(n)} = 7.36 \times 10^{-3}$. Hence, the

Please cite this article in press as: A. Kuzmin, et al., The role of the kinetic parameter in the stability of two-relaxation-time advection–diffusion lattice Boltzmann schemes, Computers and Mathematics with Applications (2010), doi:10.1016/j.camwa.2010.07.036

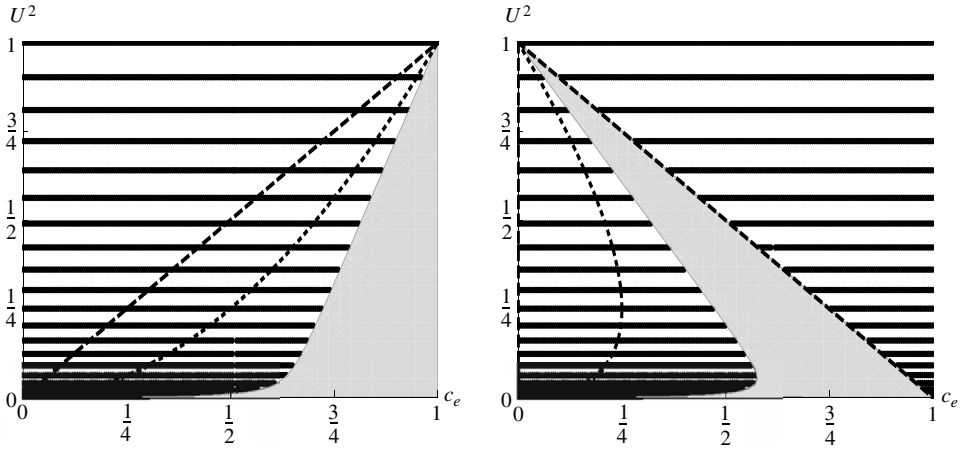

Fig. 10. Stable ("filled") areas and unstable ("dotted") subdomains are shown for the d1Q3 TRT model when $g^{(u)} = 0$ (left) and $g^{(u)} = 1$ (right). They are obtained with the help of numerical stability analysis when $\Lambda_{bgk} = 10^{-4}$ ($\tau = 0.51$) and $\Lambda = \frac{1}{12} \gg \Lambda_{bgk}$. The stable area is bounded by the stability curves constructed in this paper. For comparison, the optimal (dashed) and the non-negativity (dotted) lines are plotted. The very unstable interval c_e lies before the point of maximal curvature.

non-negativity lines do not guarantee stability (in some subinterval c_e) when $\Lambda < \Lambda^{(s)}(\Lambda_{bgk}) < \Lambda_{bgk}$, for all Λ_{bgk}. Also, they do not guarantee stability in the "unreliable zone", when $\Lambda \in [\Lambda^{(n,-)}, \Lambda^{(n,+)}] > \Lambda_{bgk}$, but only if $\Lambda_{bgk} < \Lambda^{(n)}_{bgk}$. These results are summarized in Table 4.

4. Multi-dimensional models

In this section, we examine the applicability of the d1Q3 stability curves in multi-dimensions where even Miller's approach is tedious and we mainly apply numerical stability analysis (see the details in Appendix C). We keep in mind that the stable velocity cannot be higher than the corresponding d1Q3 curve or the OTRT (necessary and sufficient) stability condition for the given equilibrium. However, the d1Q3 curves may become sufficient (until the bisection with the *d-line* boundary occurs, which is model dependent) only provided that the minimum of the stable velocity amplitude occurs for $\vec{k} \parallel \vec{U}$ when the two vectors are parallel to some coordinate axis.

The effective fourth-order corrections of the multi-dimensional advection–diffusion equations are under study (to be reported). Their preliminary analysis suggests that the models with *the same weight families*, $t_q^{(m)} = t_q^{(a)} = t_q^{(u)}$, may more easily fulfill the necessary k^4 requirements for prolonging the optimal stability on the EOTRT boundary $\Lambda = \Lambda^{(ext.)}(\Lambda_{bgk})$. The numerical stability analysis from $\tau = 0.51$ ($\Lambda^{(ext.)} \to \frac{1}{4}$) to $\tau = 100$ ($\Lambda^{(ext.)} \to \frac{1}{8}$), i.e., from $\Lambda_{bgk} = 10^{-4}$ to $\Lambda_{bgk} \approx 10^4$, confirms that both d2Q5 and d3Q7 *retain their optimal stability bounds* for the whole interval $c_e \in [0, \frac{1}{d}]$ when $\Lambda = \Lambda^{(ext.)}$. Similar results are obtained for the d3Q15$^{(stan)}$ and d3Q15$^{(unif)}$ schemes.

The results for the d2Q9 model maintain the k^4 predictions with respect to sufficiency of the advection line: the *a-line* $U^2 = 2c_e$ slightly deteriorates for the d2Q9$^{(stan)}$ model (bottom row in Fig. 11). We recall that d2Q9$^{(stan)}$ has two different weight families: $t_c^{(u)} = \frac{1}{6}$ and $t_c^{(m)} = t_c^{(a)} = \frac{1}{3}$. At the same time, the *a-line* is kept when $t_c^{(u)} = \frac{1}{3}$ or for the d2Q9$^{(unif)}$ model. The selected d2Q9 OTRT schemes do not need to imply $E_0 \geq 0$ or $E_q^+ \geq 0$. However, the *d-line* (18) is no longer sufficient beyond the OTRT subclass, especially for high diffusion coefficients (see the decreasing stability boundary in Fig. 11). The numerical analysis suggests that, modelling the isotropic tensors, the condition $E_0 \geq 0$ is sufficient for the d2Q9 model when $\Lambda < \frac{1}{4}$ but it is usually too restrictive (see Figs. 11 and 16).

In the presence of the off-diagonal equilibrium components $\sum_{\alpha,\beta} U_\alpha U_\beta c_{q\alpha} c_{q\beta}$, one cannot expect the "full" models without second-order numerical diffusion to keep the OTRT stability in the advection limit when Λ varies. However, the d3Q15 schemes may retain their OTRT stability when $\Lambda = \Lambda^{(ext.)}$, at least provided that the necessary diffusion condition (20) (which is $U^2 \leq 2c_e$ for the d3Q15$^{(stan)}$ and d3Q15$^{(unif)}$ models) dominates over the advection boundary. Indeed, this condition is satisfied provided that all the coordinate weights $\{E_q^+\}$ are non-negative: $U^2 \leq \frac{3t_c^{(m)}}{4t_d^{(u)}} c_e$ when $c_e \in [0, c_e^{(0)}]$. This constraint vanishes when $t_c^{(u)} = \frac{1}{2}$, $t_d^{(u)} = 0$, and d3Q15$^{(opt)}$ generally loses its optimal stability when $\Lambda \neq \frac{1}{4}$. Finally, the numerical observations show that the stability *may drastically drop in multi-dimensions when* $\Lambda > \frac{1}{4}$, for very small Λ_{bgk} at least, e.g., when $\Lambda_{bgk} = 10^{-4}$ and $\Lambda \geq \frac{2}{5}$. This result is quite unexpected from the one-dimensional solutions where $\Lambda \geq \frac{1}{4}$ keeps optimal stability. Since the high Λ values may also degrade the precision, we restrict the EOTRT subclass (Eq. (33)) and study of multi-dimensional models to $\Lambda < \Lambda^{(ext.)}$.

Please cite this article in press as: A. Kuzmin, et al., The role of the kinetic parameter in the stability of two-relaxation-time advection–diffusion lattice Boltzmann schemes, Computers and Mathematics with Applications (2010), doi:10.1016/j.camwa.2010.07.036

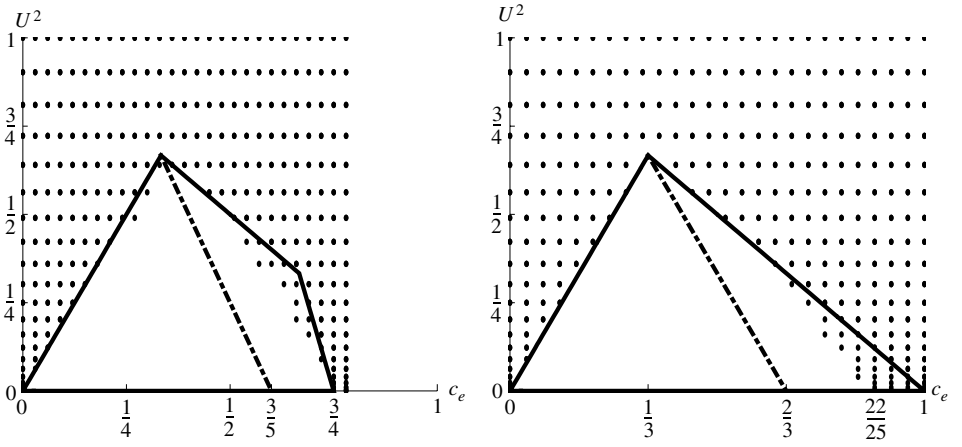

Fig. 11. The unstable area (dots) for d2Q9$^{(stan)}$ (left) and d2Q9$^{(unif)}$ (right) is shown when $\tau = 100$, $g^{(u)} = 1$, $g^{(u)}_{xy} = 0$ and $\Lambda = \Lambda^{(ext.)} \to \frac{1}{8}$. The optimal stable area is bounded by a thick solid line, given in the first column in Table 2. The E_0-*n-line* is plotted as a dotted–dashed line.

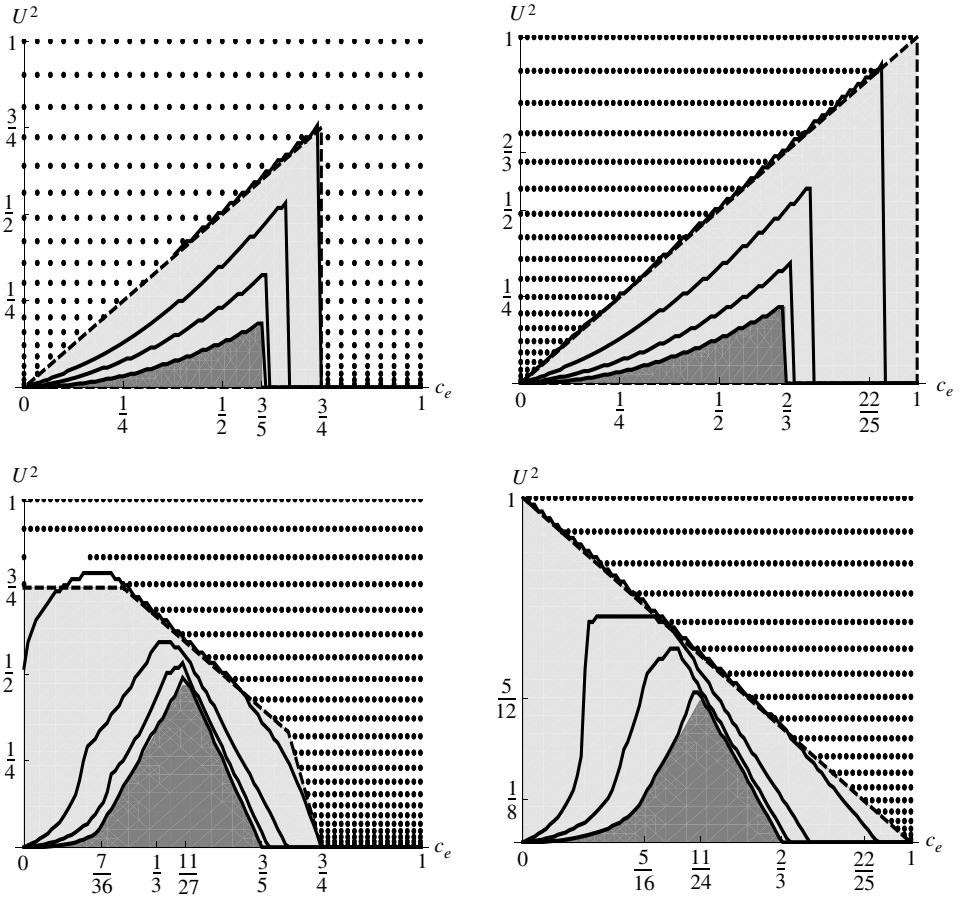

Fig. 12. Stability boundaries (solid lines) of the d2Q9$^{(stan)}$ (left) and the d2Q9$^{(unif)}$ (right) BGK models are plotted when $\tau = \frac{1}{2} + \sqrt{\frac{1}{6}} \approx 0.91$ (best solid curve) and $\tau = \{0.7, 0.6, 0.51\}$, when $g^{(u)} = 0$ (top row) and $g^{(u)}_{\alpha\beta} g^{(u)} = 1$ (bottom row). For comparison, *the unstable area* of the optimal BGK model ($\tau = 1$) is "filled" with dots and *its stable (sufficient) area* is bounded by a dashed line. The non-negativity area is dark grey.

4.1. The BGK model

We first confirm that the d2Q5, d3Q7, d2Q9$^{(stan)}$, d2Q9$^{(unif)}$ and d3Q15$^{(stan)}$, d3Q15$^{(unif)}$ BGK models converge when $\Lambda_{bgk} \to 0$ towards their respective non-negativity domains. This is demonstrated for d2Q9$^{(stan)}$ and d2Q9$^{(unif)}$ in Fig. 12:

Please cite this article in press as: A. Kuzmin, et al., The role of the kinetic parameter in the stability of two-relaxation-time advection–diffusion lattice Boltzmann schemes, Computers and Mathematics with Applications (2010), doi:10.1016/j.camwa.2010.07.036

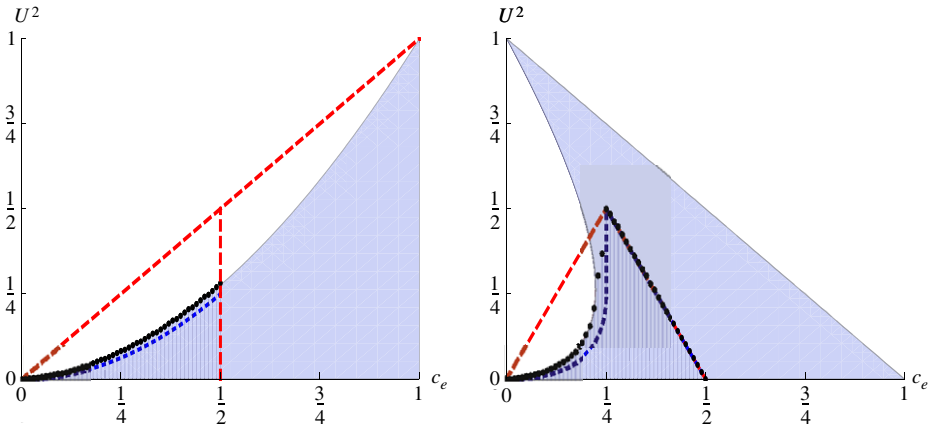

Fig. 13. The stability boundary is shown by dots for the d2Q5 BGK model with $\Lambda_{bgk} = 10^{-2}$ ($\tau = 0.6$), $g^{(u)} = 0$ (left) and $g^{(u)} = 1$ (right). The (decreasing) straight boundary segment is the E_0-*n-line*: $c_e = \frac{1}{2}$ or $U^2 = 1 - 2c_e$ for $g^{(u)} = \{0, 1\}$, respectively. For comparison, the *a-line* (dashed) of the OTRT subclass and the *n-line* (dotted) are plotted. The exact stable area of the d1Q3 model is "dashed". The d2Q5 model follows the d1Q3 stability curve until the E_0-*n-line* is reached when $g^{(u)} = 0$, and it leaves it for $c_e \approx c_e^{(c)}$ (maximal curvature point) when $g^{(u)} = 1$, then joins the E_0-*n-line* at the peak $c_e^{(p)} = \frac{1}{4}$.

the *n-line* and E_0-*n-line* are given by relations (B.5), (B.8) and (B.9) when $c_e \in [0, c_e^{(0)}]$, $c_e^{(0)} = \frac{3}{5}$ for d2Q9$^{(stan)}$ and $c_e^{(0)} = \frac{2}{3}$ for d2Q9$^{(unif)}$. Here, the BGK model with $\Lambda_{bgk} = \frac{1}{6}$ (the boundary of the extended optimal subclass $\Lambda_{bgk} = \Lambda^{(ext.)}$) keeps the optimal stability when $g^{(u)} = 0$ but loses it when $g^{(u)} g^{(u)}_{\alpha\beta} = 1$ and $c_e \to 0$, in agreement with the predictions (left bottom picture: again, this result improves when $t_c^{(u)} = \frac{1}{3}$). d2Q9$^{(unif)}$ shows larger stable areas than d2Q9$^{(stan)}$ except when $g^{(u)}_{xy} g^{(u)} = 1$ and in the limit $\Lambda_{bgk} \to 0$ where its non-negativity domain is slightly smaller. On the whole, we find that the BGK models with the same weight families (excluding $t_c^{(\cdot)} = 0$) keep the OTRT stability conditions (9) and (10) *when* $\Lambda \geq \Lambda^{(ext.)}$.

Next, we do not observe any noticeable difference between the d1Q3, d2Q5 and d3Q7 BGK solutions when $g^{(u)} = 0$ and $\Lambda < \Lambda^{(ext.)}$ (see, e.g., Fig. 13). The non-negativity condition of the minimal models $U^2 \leq c_e^2$ reduces to $U^2 \leq c_e^2/d$ for the "full" models (with equal advection and mass weights) because of the diagonal links. Hence, one cannot expect the *identical advection* behaviour of stability curves for the d1Q3 and "full" BGK models, even for $g^{(u)} = 0$. However, we find that the d1Q3 BGK curves provide very good approximations except for very small Λ_{bgk}. When $g^{(u)} = 1$, the multi-dimensional solutions may follow the d1Q3 curve only to the point of maximal curvature, or as long as they intersect their respective *d-line* boundaries.

4.2. TRT beyond the extended optimal subclass, $\Lambda < \Lambda^{(ext.)}(\Lambda_{bgk})$

The analysis of the d1Q3 TRT stability curves suggests that it is not reasonable to reduce Λ below $\Lambda^{(ext.)} \approx \frac{1}{8}$ for large Λ_{bgk} ($\Lambda_{bgk} \gg 1$). We then observe similar qualitative behaviour for all the velocity sets in the "reliable" zone, $\Lambda_{bgk}^{(crit.)} \leq \Lambda_{bgk}$, $\Lambda_{bgk}^{(crit.)} \approx 10^{-2}$ when, at least, $\Lambda^{(s)} < \Lambda < \Lambda^{(ext.)}$ and the d1Q3 stability is guaranteed by the non-negativity line. Figs. 13–15 compare the stability curves for the d2Q5 model to the d1Q3 model when $\Lambda_{bgk} = \{10^{-2}, \frac{1}{400}, 10^{-4}\}$ and $\Lambda < \Lambda^{(ext.)}(\Lambda_{bgk})$. Similar results are obtained for the d3Q7 and d3Q15$^{(stan)}$/d3Q15$^{(unif)}$ models. Fig. 16 compares the d2Q9$^{(stan)}$ and d2Q9$^{(unif)}$ stability results to exact d1Q3 curves. Here, when $\Lambda_{bgk} = 10^{-2}$ and $\Lambda = \frac{1}{8}$ (Fig. 16, top row), the stable domain is much larger than the non-negativity domain. The inverse holds when $\Lambda_{bgk} = 10^{-4}$ and $\Lambda = \frac{1}{12}$ (Fig. 16, bottom row). The effective decreasing diffusion boundary is not provided for the d2Q9 schemes beyond the OTRT but the E_0-*n-line* remains sufficient when the diffusion tensor is isotropic for all the multi-dimensional models considered.

In what follows, we use the notation $c_e \approx c_e^{(c)}$ close to the maximal curvature point of the d1Q3 stability curve and $c_e = c_e^{(p)}$ for the peak point where the *n-line* and the E_0-*n-line* meet each other for a given velocity set. When the d1Q3 stability curves are smooth enough and single-valued, where $\Lambda_{bgk} \geq \frac{1}{400}$ and $g^{(u)} = 0$, then the multi-dimensional stability boundaries follow them inside the available intervals $c_e \in [0, c_e^{(\max)}]$ (see the left diagrams in Figs. 13, 14 and 16). Moreover, the minimal models respect the d1Q3 curve even when Λ decreases below Λ_{bgk} (bottom diagrams in Fig. 14). The "full" models also follow the smooth curves (see the top left diagram in Fig. 16). When the d1Q3 curves lose their smoothness (typically, $\Lambda_{bgk} \to 0$, Λ is high), then the multi-dimensional models generally follow only the lower segment of the stability curves (left bottom diagram in Fig. 16). Recall that we suggest avoiding the interval $c_e \in [0, \approx c_e^{(c)}]$ for the sharp curves of the d1Q3 model. However, it may occur that $c_e^{(\max)} < c_e^{(c)}$ in multi-dimensions, as in Fig. 15 for $\Lambda = \frac{1}{12}$ (left bottom diagram).

Please cite this article in press as: A. Kuzmin, et al., The role of the kinetic parameter in the stability of two-relaxation-time advection–diffusion lattice Boltzmann schemes, Computers and Mathematics with Applications (2010), doi:10.1016/j.camwa.2010.07.036

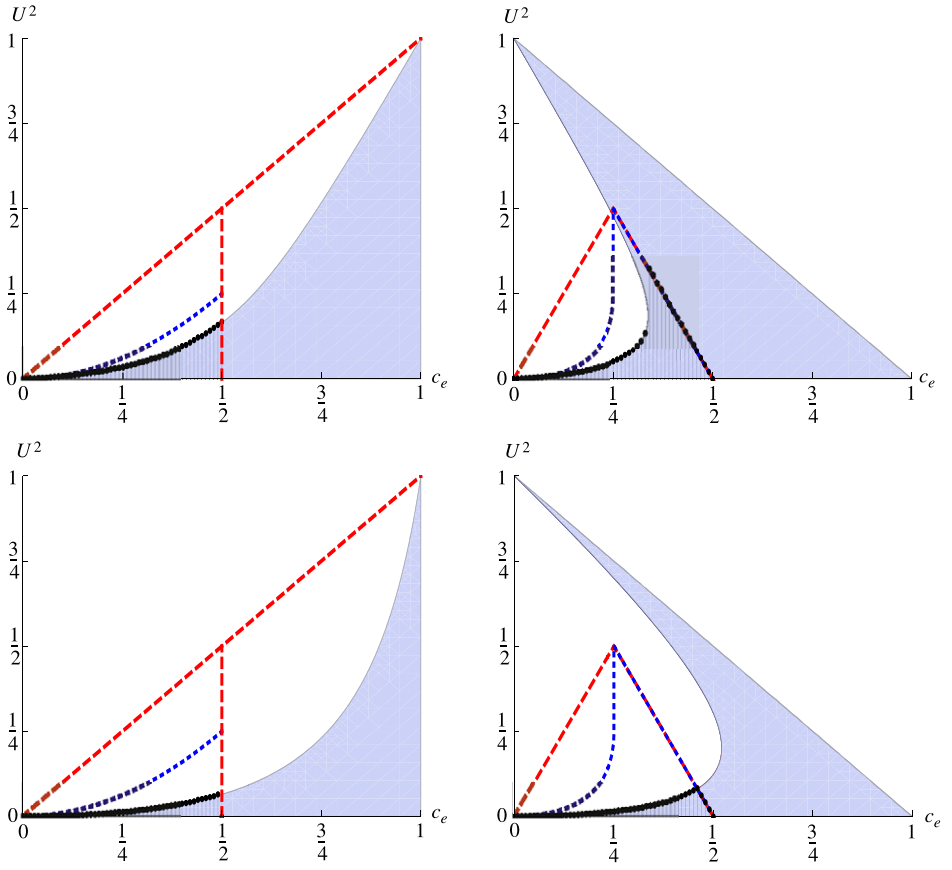

Fig. 14. Like the previous picture for the d2Q5 model but $\Lambda_{bgk} = \frac{1}{400}$ ($\tau = 0.55$): $g^{(u)} = 0$ (left) and $g^{(u)} = 1$ (right), for $\Lambda = \frac{1}{12}$ (top) and $\Lambda = 10^{-4}$ (bottom). Here, the stability boundary follows the d1Q3 stability curve until it intersects the E_0-*n-line*, except for $\Lambda = \frac{1}{12}$ (top right picture) where the E_0-*n-line* does not intersect the lower segment of the d1Q3 curve; the segment connecting to the E_0-*n-line* is (approximately) tangent to it.

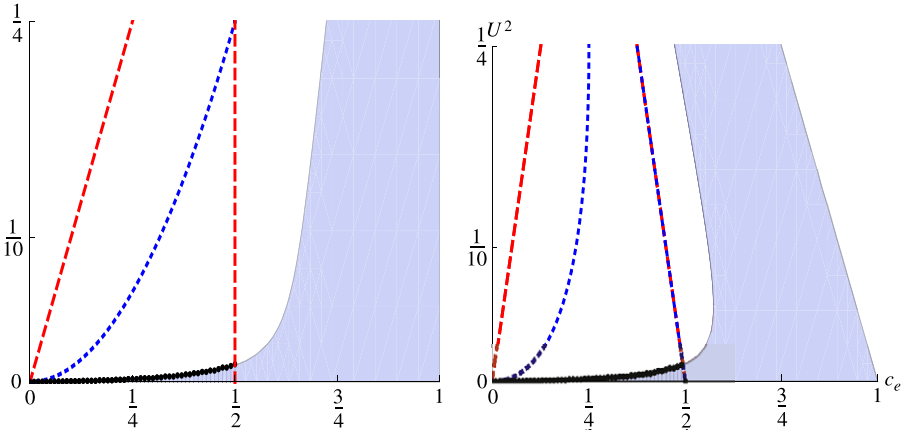

Fig. 15. Like the two previous pictures for the d2Q5 model but $\Lambda_{bgk} = 10^{-4}$ ($\tau = 0.51$) and $\Lambda = \frac{1}{12}$, within the range $U^2 \in [0, \frac{1}{4}]$. Here, $c_e^{(c)} > c_e^{(0)} = \frac{1}{2}$ and the stability boundary follows the d1Q3 curve only up to the E_0-*n-line*.

Using the one-dimensional solution can be tricky when the numerical diffusion is removed ($g^{(u)} = 1$) and the diffusion-dominant (right) stability boundaries have different forms. A particularity of the d1Q3 curves it that they join the boundary point $U^2(c_e = 0) = 1$ such that all functions $U^2(c_e)$ are double-valued. We may first distinguish the three situations for the minimal models and the d3Q15 schemes. First, when $c_e^{(c)} < c_e^{(p)}$ (right diagram in Fig. 13) then the stability boundary follows the d1Q3 curve as long as $c_e \approx c_e^{(c)}$; then it joins the E_0-*n-line* at $c_e = c_e^{(p)}$. Second, inversely, when $c_e^{(p)} < c_e^{(c)}$ and the E_0-*n-line* intersects the lower segment of the d1Q3 curve (bottom right diagrams in Figs. 14 and 15), then the stability

Please cite this article in press as: A. Kuzmin, et al., The role of the kinetic parameter in the stability of two-relaxation-time advection–diffusion lattice Boltzmann schemes, Computers and Mathematics with Applications (2010), doi:10.1016/j.camwa.2010.07.036

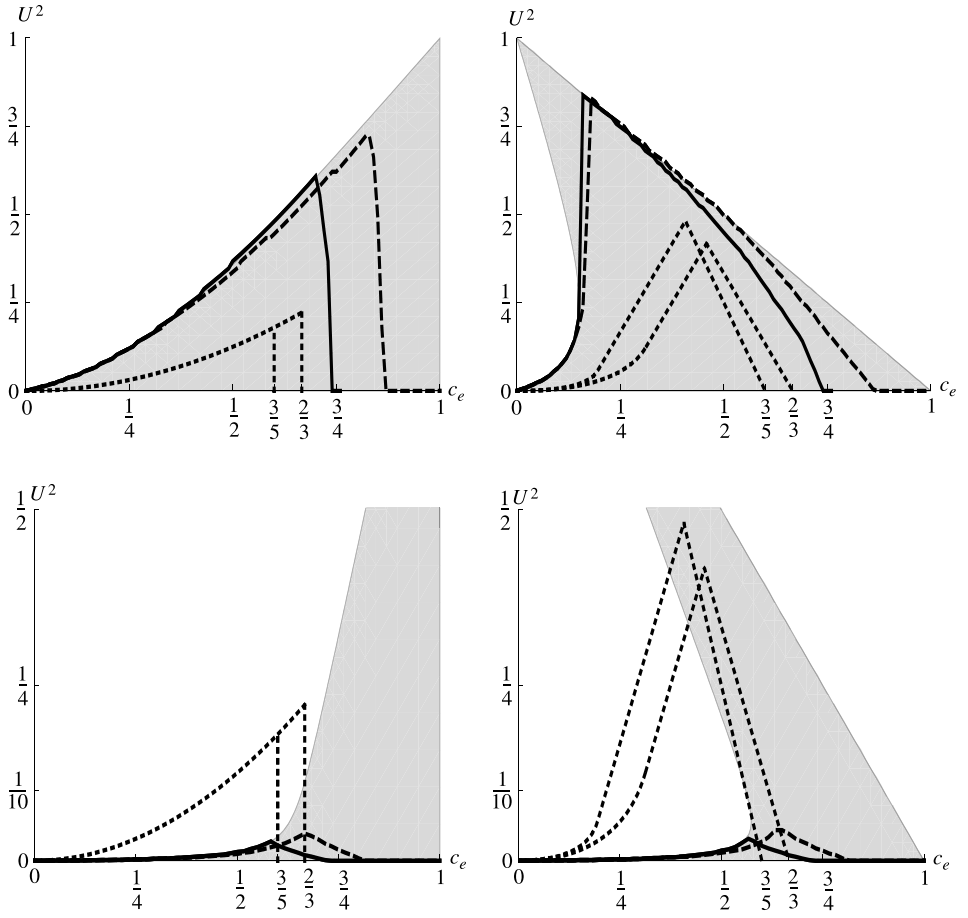

Fig. 16. The stability boundary is shown for d2Q9$^{(stan)}$ (solid line) and d2Q9$^{(unif)}$ (dashed line) when $g^{(u)} = 0$ (left) and $g^{(u)}_{xy} g^{(u)} = 1$ (right), for $\Lambda_{bgk} = 10^{-2}$ ($\tau = 0.6$), $\Lambda = \frac{1}{8}$ (top row) and $\Lambda_{bgk} = 10^{-4}$ ($\tau = 0.51$), $\Lambda = \frac{1}{12}$ (bottom row). The stable domain of the d1Q3 model is "filled". The non-negativity domain of each model is bounded by a dotted line, with $c_e^{(0)} = \frac{3}{5}$ for d2Q9$^{(stan)}$ and $c_e^{(0)} = \frac{2}{3}$ for d2Q9$^{(unif)}$. When $g^{(u)}_{xy} g^{(u)} = 1$, the stability curves leave the d1Q3 solution when $c_e <\approx c_e^{(c)}$.

boundary follows the one-dimensional curve up to its intersection with the E_0-*n-line*. This is similar to the $g^{(u)} = 0$ case, with a possible departure from the "sharp" curve. Finally, the intermediate case is the most difficult: when $c_e^{(p)} < c_e^{(c)}$ but the E_0-*n-line* does not intersect the lower segment of the d1Q3 curve (the top right diagram in Fig. 14). In such a case, it is difficult to prescribe the slope of the connecting segment towards the E_0-*n-line*.

In summary, the d1Q3 stability curves turn out to be useful in multi-dimensions: they provide the necessary advection conditions. The d1Q3, d2Q5 and d3Q7 BGK models have very similar (or the same) low segments of advection boundaries $U^2(c_e, \Lambda_{bgk}, \Lambda)$. As a first approximation, one can follow the d1Q3 stability curve up to intersection with the E_0-*n-line*. This is also valid for the selected "full" models, like d2Q9$^{(stan)}$/d2Q9$^{(unif)}$ or d3Q15$^{(stan)}$/d3Q15$^{(unif)}$. If the d1Q3 curve has a very large curvature, one should expect the one-dimensional predictions to be reliable only before its point of maximum. The stability scenario can be predicted for $g^{(u)} = 1$ when the E_0-*n-line* intersects the lower segment of the d1Q3 curve before it bends. Otherwise, one obtains some ideas connecting the maximum curvature point with the non-negativity peak or the E_0-*n-line* such that $U^2(c_e)$ remains single-valued.

5. Concluding remarks

This work further investigates the role of free collision rate in the stability of the TRT operator for the ADE. We extend the methodology of [23], first to delineate the principal necessary advection-dominant and diffusion-dominant conditions, then to perform the exact von Neumann stability analysis of the linear TRT operator with the help of Miller's theory [25]. The necessary advection conditions (9)–(10) guarantee the positive semi-definiteness of the effective diffusion tensor for isotropic problems. The necessary diffusion-dominant conditions restrict the symmetric equilibrium weights to a general form given by relations (17)–(20). All of these conditions have to be respected by any LBE ADE model.

Please cite this article in press as: A. Kuzmin, et al., The role of the kinetic parameter in the stability of two-relaxation-time advection–diffusion lattice Boltzmann schemes, Computers and Mathematics with Applications (2010), doi:10.1016/j.camwa.2010.07.036

In this paper, we build the exact stability bounds of the d1Q3 TRT ADE model. Above all, this shows that the stability is generally not controlled by the "magic" parameter $\Lambda = \Lambda^-\Lambda^+$ but depends on a pair of eigenvalue functions, say $\Lambda_{bgk} = (\Lambda^-)^2$ and Λ, in agreement with the predictions of the *time-dependent* recurrence equations of the TRT operator [16]. Only two exceptions have been found so far. The first one is the so-called OTRT subclass $\Lambda = \frac{1}{4}$ where the stability bounds no longer depend on eigenvalues for any velocity set and any equilibrium [23]. The second one, *extended optimal* EOTRT subclass, is derived in this work. The EOTRT subclass expands the OTRT subclass to the larger interval $\Lambda \geq \Lambda^{(ext.)}(\Lambda_{bgk}) > \frac{1}{8}$ where the d1Q3 model retains optimal stability. The BGK model benefits from this extension when $\Lambda_{bgk} \geq \frac{1}{6}$, penalizing the high Peclet numbers. The minimal models and the "full" models with the same weights, $t_q^{(m)} = t_q^{(a)} = t_q^{(u)}$, are good candidates for keeping the optimal stability in the advection limit, at least on the boundary $\Lambda = \Lambda^{(ext.)}$. Hence, the OTRT subclass and, partially, the EOTRT subclass, possess the most favourable equilibrium stability conditions—the same for all Peclet numbers when the equilibrium is set. The optimal stability conditions are easier and less restrictive than the non-negativity condition of equilibrium distributions.

Beyond the EOTRT subclass, when $\Lambda < \Lambda^{(ext.)}(\Lambda_{bgk})$, one should be very careful with the choice of Λ. We first identify "reliable" and "unreliable" choices for Λ_{bgk}. The reliable choice $\Lambda_{bgk} \geq\approx 10^{-2}$ is more stable than its BGK counterpart when $\Lambda > \Lambda_{bgk}$, and less stable only when $\Lambda < \Lambda_{bgk}$. We then derive the necessary and sufficient intervals for $\Lambda(\Lambda_{bgk})$ where the stability is still guaranteed by the non-negativity conditions. Decreasing $\Lambda \sim \alpha\Lambda_{bgk}$ when $\Lambda_{bgk} \to 0$ one either gets the BGK ($\alpha = 1$) or loses against it in stability. Yet, one could advocate the BGK model in the "unreliable" zone for its simple stability control by the non-negativity curves, with no danger of losing their sufficiency for "improper" choices of free eigenvalue. We suggest that a reasonable strategy for the TRT model is to select a suitable Λ value for the (predicted) variation of Λ_{bgk} and to set it. This will reduce the inconsistency of the variation of the spatial truncated errors with the diffusion coefficients and improve their accuracy, especially for large Λ_{bgk}. However, the most suitable stability interval $\Lambda^{(ext.)} \leq \Lambda \leq \frac{1}{4}$ then rapidly approaches $\Lambda = \frac{1}{4}$ when $\Lambda_{bgk} \to 0$.

On the whole, this study encourages us to continue the work with and related to the TRT model. The principal one-dimensional guidelines on the choice of the suitable pair (Λ_{bgk}, Λ) are valid in multi-dimensions when $\Lambda < \frac{1}{4}$. The combinations of high values $\Lambda_{bgk} \gg 1$ with small $\Lambda \leq \frac{1}{8}$ should be avoided. We also observe that the combinations of small Λ_{bgk} values with $\Lambda > \frac{1}{4}$ may drastically reduce the stable areas in multi-dimensions. The work in progress is intended to confirm these observations, to extend the necessary and sufficient stability conditions to anisotropic diffusion tensors and to find a compromise between accuracy and stability. The next interesting research aim is to understand the reasons for the observed stability drop in practical computations (boundaries, non-linearities), first examining them for the OTRT subclass. Finally, the MRT operators reduce to the TRT on the d1Q3 velocity set but they possess more "ghost" eigenvalues in multi-dimensions.

Acknowledgements

A. Kuzmin wishes to thank Alberta Ingenuity Fund for their financial support. I. Ginzburg is grateful to Calgary University for hospitality. The authors are grateful to D. d'Humières for much advice, and L. Hills and T. Reis for proofreading assistance.

Appendix A. Stability curves of the d1Q3 model: details

A.1. The characteristic equation of the d1Q3 model

The characteristic third-order equation with respect to Ω has the form (26) where $\mathcal{D}^+_{\alpha\alpha} = c_e + g^{(u)}U^2$ and $s^- = U$. When $g^{(u)} = 0$, the solution of the linear equation with the equivalent (in the von Neumann sense) stability properties is

$$g^{(u)} = 0 : |\Omega(c_e, U^2, \Lambda_{bgk}, \Lambda, m)|^2 = \frac{P_n(U^2)}{P_d(U^2)},$$

where

$$\begin{aligned}
&P_n(U^2) = a_n + b_nU^2 + c_nU^4,\\
&a_n = (2\Lambda_m\bar{\Lambda} + c_m\Lambda_b\Lambda)^2(2\bar{\Lambda}(\bar{c}_m + 4\Lambda) - c_m\Lambda_l\Lambda_{bgk})^2,\\
&b_n = 2m(4\bar{\Lambda}^2 - \Lambda_l^2\Lambda^2)(2\bar{\Lambda}(\bar{c}_m + 4\Lambda) - c_m\Lambda_l\Lambda_{bgk})\\
&\qquad \times(\Lambda(1 + c_m + 4m\Lambda) + \Lambda_{bgk}(1 + 4\bar{c}_m\Lambda)) + 4m(4\bar{\Lambda}^2(\bar{c}_m + 4\Lambda) + c_m\Lambda_l^2\Lambda\Lambda_{bgk})^2,\\
&c_n = m^2(4\bar{\Lambda}^2 - \Lambda_l^2\Lambda^2)^2,
\end{aligned}$$

and

$$\begin{aligned}
&P_d(U^2) = a_d + b_dU^2 + c_dU^4,\\
&a_d = (2\Lambda_m\bar{\Lambda} + c_m\Lambda_b\Lambda)^2(2\bar{\Lambda}(m + 4\Lambda) - c_m\Lambda_b\Lambda)^2,\\
&b_d = -2m(4\Lambda^2 - \Lambda_{bgk})^2(2\Lambda_m\bar{\Lambda} + c_m\Lambda_b\Lambda)(8\bar{\Lambda}\Lambda + \bar{c}_m\Lambda + m\Lambda_c\Lambda_{bgk}),\\
&c_d = m^2(4\Lambda^2 - \Lambda_{bgk})^4,
\end{aligned}$$

with

$$m = \tan^2\left(\frac{k}{2}\right), \quad \bar{\Lambda} = \frac{(\Lambda + \Lambda_{bgk})}{2}, \quad c_m = mc_e, \quad \bar{c}_e = 1 - c_e, \quad \bar{c}_m = m\bar{c}_e,$$
$$\Lambda_l = 1 + 4\Lambda, \quad \Lambda_m = 1 + 4m\Lambda, \quad \Lambda_c = 1 + 4c_e\Lambda, \quad \Lambda_b = 1 - 4\Lambda_{bgk}. \tag{A.1}$$

When $U = 0$, the sufficient stability condition $|\Omega|^2 \le 1\ \forall\ m > 0$ becomes

$$8c_e\Lambda_{bgk}\bar{\Lambda}(1 + 4\Lambda)m((c_e - 1)m - 4\Lambda) \le 0, \quad \forall\ m > 0. \tag{A.2}$$

This condition is satisfied when $c_e \in [0, \min_{m>0} \frac{(4\Lambda+m)}{m}]$, hence

$$c_e \in [0, 1], \quad \forall\ \{\Lambda, \Lambda_{bgk}\}. \tag{A.3}$$

The minimum corresponds to $m = \infty$ ($k = \pi$). Hence, the condition (A.3), or $U^2 \le 1 - c_e$ when $g^{(u)} = 1$, is necessary ($\forall\ U$) and sufficient (when $U \equiv 0$) for the d1Q3 TRT model with any eigenvalues, in agreement with the diffusion-dominant condition $E_0 \ge 0$. Using solution (28) for $|\Omega|^2$ when $\Lambda = \frac{1}{4}$ and $g^{(u)} = 0$, $|\Omega|^2 \le 1$ if

$$(c_e^2 m - c_e(1 + m) + U^2) \le 0, \quad 0 \le c_e \le 1, \tag{A.4}$$

then, necessarily,

$$0 \le U^2 \le c_e \min_{m>0}\{1 + m(1 - c_e)\} = c_e, \quad 0 \le c_e \le 1. \tag{A.5}$$

This condition corresponds to the "advection" limit $m \to 0$. Again, replacing c_e with $c_e + U^2$ for $g^{(u)} = 1$, one obtains the optimal conditions (25) for this case. Fourth-order expansion of relation (28) with the coefficients (A.1) in the advection limit $k \to 0$ yields

$$|\Omega|^2 = 1 - \frac{C_e\Lambda_{bgk}\Lambda_l k^2}{8\Lambda\bar{\Lambda}} + \frac{\Lambda_l k^4}{512\Lambda^2\bar{\Lambda}^3}(a_s C_e + (b_s C_e - k_s)U^2 + k_s U^4) + O(k^6),$$

where

$$C_e = c_e - U^2, \quad \bar{\Lambda} = \frac{(\Lambda + \Lambda_{bgk})}{2}, \quad \Lambda_l = 1 + 4\Lambda,$$
$$a_s = \frac{2}{3}\Lambda_{bgk}\bar{\Lambda}(2\bar{\Lambda}(3 - 8\Lambda) + 3C_e(\Lambda_{bgk} - (1 - 8\Lambda_{bgk})\Lambda)),$$
$$b_s = \Lambda_{bgk}\Lambda^2(32\Lambda^2 - 4\Lambda - 1) - 4\Lambda^4 + \Lambda_{bgk}^2\Lambda(80\Lambda^2 + 12\Lambda - 1) + \Lambda_{bgk}^3(32\Lambda^2 + 4\Lambda - 1),$$
$$k_s = 16\Lambda\bar{\Lambda}^2(\Lambda(4\Lambda - 1) + \Lambda_{bgk}(8\Lambda - 1)). \tag{A.6}$$

Then, clearly, $C_e \ge 0$ is the necessary k^2 condition (*a-line*) for supporting $|\Omega|^2 \le 1$. Plugging $C_e = 0$ into the coefficient of k^4 we obtain

$$|\Omega|^2 = 1 + \frac{(4\Lambda + 1)k^4}{32\Lambda^2\bar{\Lambda}^3}k_s U^2(U^2 - 1) + O(k^6). \tag{A.7}$$

Again taking into account the necessary conditions (25), the coefficient of k^4 is negative only if $k_s \ge 0$, i.e., only if Λ_{bgk} and Λ satisfy conditions (30).

A.2. The BGK stability curves

The solution U_0^2 of the minimization problem (29) for the BGK case with $\Lambda_{bgk} \le \frac{1}{6}$ is given by a suitable (non-negative, with $U^2(c_e = 1) = 1$ and $U^2(\Lambda_{bgk} \to 0) = c_e^2$) root of the third-order equation (34) where the coefficients $\{a_{i,j}(\Lambda_{bgk}) = a_{i,j}(\Lambda_{bgk}, \Lambda_{bgk})\}$ of the fifth-order polynomials $\{a_i(c_e)\}$ are given by the following sets, from $j = 0$ to $j = 5$:

$$a_0 = \{0, -128\Lambda_b^3\Lambda_{bgk}, 16\Lambda_b^2(32\Lambda_d\Lambda_{bgk} - 1), -48\Lambda_b\Lambda_d(16\Lambda_d\Lambda_{bgk} - 1), 16\Lambda_d^2(32\Lambda_d\Lambda_{bgk} - 3), 16\Lambda_b\Lambda_d^3\};$$
$$a_1 = \{16\Lambda_b^2\Lambda_d^2, 16\Lambda_b(16\Lambda_{bgk}(1 + \Lambda_{bgk}(6\Lambda_{bgk} - 5)) - 3),$$
$$8(5 + 2\Lambda_{bgk}(2\Lambda_{bgk}(79 + 16\Lambda_{bgk}(11\Lambda_{bgk} - 18)) - 21)),$$
$$8\Lambda_b\Lambda_{bgk}(7 + 16\Lambda_{bgk}(3\Lambda_{bgk} - 8)), 4\Lambda_b^2((\Lambda_{bgk} - 10)\Lambda_{bgk} - 2), 0\};$$
$$a_2 = \{8\Lambda_d^2(1 + 8\Lambda_d\Lambda_{bgk}), -8\Lambda_b(2 + \Lambda_{bgk}(11 + 8\Lambda_{bgk}(4\Lambda_{bgk} - 5))),$$
$$+ \Lambda_b^2(7 + 4\Lambda_{bgk}(15 - 2\Lambda_{bgk})), \Lambda_b^3, 0, 0\};$$
$$a_3 = \{\Lambda_b^2\Lambda_d^2, -\Lambda_b^3, 0, 0, 0, 0\}, \quad \text{where } \Lambda_b = 1 - 4\Lambda_{bgk}, \Lambda_d = 1 - 2\Lambda_{bgk}. \tag{A.8}$$

Please cite this article in press as: A. Kuzmin, et al., The role of the kinetic parameter in the stability of two-relaxation-time advection–diffusion lattice Boltzmann schemes, Computers and Mathematics with Applications (2010), doi:10.1016/j.camwa.2010.07.036

Fig. 4 plots several solutions to Eq. (34) with coefficients (A.8). The slopes of the stability curves when $g^{(u)} = 0$ and $\Lambda_{bgk} \leq \frac{1}{6}$ are

$$U_0^{'}(\Lambda_{bgk}) = \frac{\partial U^2}{\partial c_e}(c_e = 0) = \frac{8(1-4\Lambda_{bgk})\Lambda_{bgk}}{(1-2\Lambda_{bgk})^2}, \tag{A.9}$$

$$U_1^{'}(\Lambda_{bgk}) = \frac{\partial U^2}{\partial c_e}(c_e = 1) = \frac{1+4\Lambda_{bgk}(1-4\Lambda_{bgk}) - \sqrt{1+8\Lambda_{bgk}(1-6\Lambda_{bgk})}}{8\Lambda_{bgk}^2}. \tag{A.10}$$

The function $U_0^{'}(\Lambda_{bgk})$ monotonically increases from 0 (the *n-line*'s slope) to 1 (the *a-line*'s slope) when Λ_{bgk} increases from 0 to $\frac{1}{6}$. Accordingly, $U_1^{'}(\Lambda_{bgk})$ monotonically decreases from 2 to 1. The slope functions can be used for spline approximations of exact stability curves; e.g., a simple linear interpolation with the weight factor $w = U_0^{'}(\Lambda_{bgk})$ for c_e and $1-w$ for c_e^2 gives sufficient conditions when $g^{(u)} = 0$.

A.3. The TRT stability curves

When $\Lambda \geq \Lambda^{(ext.)}$, the optimal conditions (25) are necessary and sufficient for any Λ_{bgk}. The solution U_0^2 of the minimization problem (29) for the TRT model with $\Lambda \in]0, \Lambda^{(ext.)}(\Lambda_{bgk})]$ and $\forall\ \Lambda_{bgk} > 0$ is given by a suitable (non-negative, with $U^2(c_e = 1) = 1$) root of the third-order equation (34), where the coefficients $\{a_{i,j}(\Lambda_{bgk}, \Lambda)\}$ of the fifth-order polynomials $\{a_i(c_e)\}$ are given by the following sets, from $j = 0$ to $j = 5$:

$$\begin{aligned}
a_0 = {} & \frac{\bar{\Lambda}\Lambda}{\Lambda_{bgk}^5}\{0, -128\bar{\Lambda}^4\Lambda_a^3, 16\bar{\Lambda}^3\Lambda_a^2(16\Lambda_k - 1), 24\Lambda_k\bar{\Lambda}^2\Lambda_a(1-8\Lambda_k), 16\Lambda_g^2\bar{\Lambda}(16\Lambda_k - 3), 16\Lambda_b\Lambda_g^3\};\\
a_1 = {} & \frac{1}{\Lambda_{bgk}^6}\{16\bar{\Lambda}^4\Lambda_a^2(\bar{\Lambda} - 2\Lambda^2)^2, -8\bar{\Lambda}^3\Lambda_a(\Lambda_{bgk}^3\Lambda_a + \Lambda(\Lambda(2\Lambda_{bgk}(1-8\Lambda(1+\Lambda(12\Lambda-5))) + \Lambda\Lambda_a^2)\\
& + 2\Lambda_{bgk}^2(1 - 2\Lambda + 32\Lambda^2))), 2\bar{\Lambda}^2(3\Lambda_{bgk}^4\Lambda_a^2 + \Lambda(6\Lambda_{bgk}^3(1 + 32(1-6\Lambda)\Lambda^2)\\
& + \Lambda(6\Lambda_{bgk}\Lambda + \Lambda_{bgk}^2(2 + 4\Lambda(16\Lambda(7 + 4\Lambda(11\Lambda - 9)) - 9)) + 3\Lambda^2(\Lambda_a^2 - 4\Lambda_{bgk}(7 - 44\Lambda + 96\Lambda^2))))),\\
& - 2\bar{\Lambda}(\Lambda_{bgk}^5\Lambda_a^2 + \Lambda(2\Lambda_{bgk}^4(1 + 2\Lambda(3 + 4(3 - 32\Lambda)\Lambda))\\
& + \Lambda(\Lambda_{bgk}^3(4\Lambda(5 + 4\Lambda(7 + 16\Lambda(3\Lambda - 4))) - 3) - 3\Lambda_{bgk}^2\Lambda\\
& + \Lambda^2(\Lambda + \Lambda_{bgk}(2 - 36\Lambda\Lambda_a) - 4(\Lambda_{bgk}^2(3 + 4\Lambda(-19 + 44\Lambda)) + \Lambda^2))))),\\
& \frac{1}{4}(\Lambda_{bgk}^6 + 2\Lambda_b\Lambda_{bgk}^5\Lambda + \Lambda_{bgk}^2\Lambda^4(8\Lambda_{bgk}(9 + 4\Lambda_{bgk}(1 - 20\Lambda_{bgk})) - 9)\\
& + 2\Lambda_{bgk}\Lambda^5(1 - 8\Lambda_{bgk}(1 + 2\Lambda_{bgk}(40\Lambda_{bgk} - 11))) + \Lambda_{bgk}^4\Lambda^2(8\Lambda_{bgk}(3 + 2\Lambda_{bgk}) - 9)\\
& + \Lambda_b^2\Lambda^6(1 + 8\Lambda_{bgk}(2\Lambda_{bgk} - 5)) + 4\Lambda_{bgk}^3\Lambda^3(2\Lambda_{bgk}(9 + 4\Lambda_{bgk}) - 5)), 0\},
\end{aligned} \tag{A.11}$$

and

$$\begin{aligned}
a_2 = {} & \frac{\Lambda}{\Lambda_{bgk}^6}\{8\bar{\Lambda}^2(\bar{\Lambda} - 2\Lambda^2)^2(\Lambda_{bgk}(1+4\Lambda) + 4\Lambda_a\Lambda^2), -\bar{\Lambda}(3\Lambda_l\Lambda_{bgk}^4 + \Lambda(\Lambda_{bgk}^3(5 + 4\Lambda(3 - 40\Lambda))\\
& + \Lambda_{bgk}^2\Lambda(5 + 16\Lambda(4\Lambda(11\Lambda - 4) - 1)) + 12\Lambda_a^2\Lambda^4 + \Lambda_{bgk}\Lambda^2(3 + 4\Lambda(1 - 8\Lambda(5 + 4\Lambda(8\Lambda - 5)))))),\\
& 6\Lambda_a\Lambda^6 + \frac{1}{2}(3\Lambda_l\Lambda_{bgk}^5 + 4\Lambda_{bgk}^4\Lambda(1 + \Lambda(3 - 44\Lambda)) + \Lambda_{bgk}\Lambda^4(3 + 4\Lambda(4\Lambda(32\Lambda - 9) - 1))\\
& + 12\Lambda_{bgk}^3\Lambda^3(4\Lambda(12\Lambda - 5) - 1) - 4\Lambda_{bgk}^2\Lambda^3(\Lambda(3 + 4\Lambda(9 + 4\Lambda(4\Lambda - 15))) - 1)),\\
& \frac{1}{2}(\Lambda_{bgk}\Lambda^2(8\Lambda^3(\Lambda_b - 8\Lambda_{bgk}^2) + 4\Lambda_{bgk}^2 - \Lambda^2(1 + 16\Lambda_{bgk}))\\
& - 4\Lambda^3(\Lambda^3(1 + 16\Lambda_{bgk}(\Lambda_{bgk} - 1)) - 2\Lambda_{bgk}^3(8\Lambda_{bgk} - 1)) - \Lambda_l\Lambda_{bgk}^5), 0, 0\}
\end{aligned}$$

$$a_3 = \frac{(\Lambda_{bgk} - 4\Lambda^2)^2\Lambda^2}{4\Lambda_{bgk}^6}\{4(\bar{\Lambda} - 2\Lambda^2)^2, -2(\Lambda_{bgk}^2 + \Lambda^2(1 - 8\bar{\Lambda})), (\Lambda_{bgk} - \Lambda)^2, 0, 0, 0\};$$

where

$$\begin{aligned}
& \bar{\Lambda} = \frac{(\Lambda + \Lambda_{bgk})}{2}, \quad \Lambda_l = 1 + 4\Lambda, \quad \Lambda_a = 1 - 4\Lambda, \quad \Lambda_b = 1 - 4\Lambda_{bgk},\\
& \Lambda_k = \Lambda_{bgk}\Lambda_a + \Lambda, \quad \Lambda_g = \bar{\Lambda} - 2\Lambda_{bgk}\Lambda.
\end{aligned} \tag{A.12}$$

When $\Lambda = \Lambda_{bgk}$, this set reduces to relations (A.8), with $a_{i,j}(\Lambda_{bgk}) = a_{i,j}(\Lambda_{bgk}, \Lambda_{bgk})$. When $g^{(u)} = 0$ and $\Lambda \leq \Lambda^{(ext.)}(\Lambda_{bgk})$ the boundary slopes of the stability curves are

$$U_0^{'}(\Lambda_{bgk}, \Lambda) = \frac{8\Lambda_{bgk}\Lambda\bar{\Lambda}(1-4\Lambda)}{(\bar{\Lambda} - 2\Lambda^2)^2}, \quad \bar{\Lambda} = \frac{(\Lambda + \Lambda_{bgk})}{2}, \quad \Lambda \leq \Lambda^{(ext.)}(\Lambda_{bgk}),$$

Please cite this article in press as: A. Kuzmin, et al., The role of the kinetic parameter in the stability of two-relaxation-time advection–diffusion lattice Boltzmann schemes, Computers and Mathematics with Applications (2010), doi:10.1016/j.camwa.2010.07.036

and then

$$
\begin{aligned}
&U_0' \to 1, \quad \text{when } \Lambda \to \Lambda^{(ext.)}(\Lambda_{bgk}), \forall\ \Lambda_{bgk} > 0,\\
&U_0' \to 0, \quad \text{when } \Lambda = \Lambda_{bgk} \to 0,\\
&U_0' \to 0, \quad \text{when } \Lambda_{bgk} \to 0,\\
&U_0' \to 0, \quad \text{when } \Lambda \to 0,\ \forall\ \Lambda_{bgk} > 0.\\
&U_1'(\Lambda_{bgk}, \Lambda) = \frac{1}{8\Lambda^3}(2\Lambda^2(1-8\Lambda_{bgk}) + (1+2\Lambda)\Lambda_{bgk})\\
&\qquad\qquad - \frac{1}{8\Lambda^3}\sqrt{(1-4\Lambda)\Lambda_{bgk}(\Lambda_{bgk} + 4\Lambda(\Lambda+2\Lambda_{bgk}))}, \quad \Lambda \le \Lambda^{(ext.)}(\Lambda_{bgk}),
\end{aligned}
\tag{A.13}
$$

and then

$$
\begin{aligned}
&U_1' \to 1, \quad \text{when } \Lambda \to \Lambda^{(ext.)}(\Lambda_{bgk}),\ \forall\ \Lambda_{bgk} > 0,\\
&U_1'(\alpha) \to \frac{1+6\alpha+\alpha^2}{4\alpha}, \quad \text{when } \Lambda = \alpha\Lambda_{bgk},\ \Lambda_{bgk} \to 0,\\
&U_1' \to 2 = \min_{\alpha} U_1'(\alpha), \quad \text{when } \Lambda = \Lambda_{bgk} \to 0,\\
&U_1' \to \frac{1}{4\Lambda}, \quad \text{when } \Lambda \ne \Lambda_{bgk},\ \Lambda_{bgk} \to 0,\\
&U_1' \sim \frac{\Lambda_{bgk}}{4\Lambda}, \quad \text{when } \Lambda \ne \Lambda_{bgk},\ \Lambda \to 0.
\end{aligned}
\tag{A.14}
$$

These slope functions reduce to relations (A.9) and (A.10) when $\Lambda = \Lambda_{bgk}$, with $U_0'(\Lambda_{bgk}) = U_0'(\Lambda_{bgk}, \Lambda_{bgk})$ and $U_1'(\Lambda_{bgk}) = U_1'(\Lambda_{bgk}, \Lambda_{bgk})$. They can be obtained with the help of a series expansion over c_e for root $U^2(c_e, m)$ of the quadratic equation $P_d(U^2) = P_n(U^2)$, and then taking, respectively, their minimum and maximum over m for $c_e = 0$ and $c_e = 1$, with no use of an exact solution. It appears that $U_0'(\Lambda_{bgk}, \Lambda)$ is monotonic with Λ, i.e., $U_0'(\Lambda_{bgk}, \Lambda) < U_0'(\Lambda_{bgk}, \Lambda_{bgk})$ only when $\Lambda < \Lambda_{bgk}$. The slope function $U_1'(\Lambda_{bgk}, \Lambda)$ is not monotonic with Λ and is related to the complex behaviour of the stability curves in Section 3.4.

Appendix B. Non-negativity conditions

B.1. The necessary condition for minimal BGK models when $\tau \to \frac{1}{2}$

In this section, we discuss the particular solution for $\vec{k}$ and the equilibrium parameters $\{E_q^+, E_q^-\}$ which give $|\Omega|^2 = 1$ as the solution to the characteristic equation (26) in the particular limit $\Lambda_{bgk} \to 0$ of the BGK model. This solution necessarily prescribes the non-negativity condition $\{E_q \ge 0\}$ for the minimal models. The solution to characteristic equation (26) is given by relations (28) and (A.1). It is valid for all the velocity sets when $\vec{k} = k\vec{1}_\alpha$, and also for the minimal models when $\vec{k} = k\vec{1}_d$ (diagonal direction), replacing U^2 with $(s^-)^2$ and c_e with s^+:

$$
\begin{aligned}
&\vec{k} = k\vec{1}_\alpha, \quad \text{all models}: \ s^+ = \sum_{q:c_{q\alpha}\ne 0} E_q^+ = \sum_{q=1}^{Q_m} E_q^+ c_{q\alpha}^2 = \mathcal{D}_{\alpha\alpha}^+,\\
&s^- = \sum_{q=1:c_{q\alpha}\ne 0}^{Qm/2} (E_q^- - E_{\bar{q}}^-) = \pm \sum_{q=1}^{Q_m} t_q^{(a)} \sum_{\beta} U_\beta c_{q\beta} c_{q\alpha} = \pm U_\alpha,\\
&\vec{k} = k\vec{1}_d, \quad \text{minimal models}: \ s^+ = \sum_{q=1}^{Q_m} E_q^+ = 1 - E_0,\\
&s^- = \sum_{q=1}^{Q_m/2} (E_q^- - E_{\bar{q}}^-) = \pm \sum_{q=1}^{Q_m} \sum_{\alpha} t_q^{(a)} U_\alpha c_{q\alpha}^2 = \pm \sum_{\alpha} U_\alpha.
\end{aligned}
\tag{B.1}
$$

Diffusion-dominant conditions [23] for $\vec{k} = \pi\vec{1}_\alpha$ and $\vec{k} = \pi\vec{1}_d$ constrain s^+ to $[0, 1]$. Then, plugging the BGK relation $\Lambda = \Lambda_{bgk}$ into solution (A.1) (or directly into Eqs. (26), and then performing Miller's construction (27) twice for the BGK operator), and finally taking the limit $\Lambda_{bgk} \to 0$, we obtain the following solution:

$$
\text{BGK}, \ \Lambda_{bgk} \to 0 : |\Omega|^2 = \frac{P_n(s^+, (s^-)^2)}{P_d(s^+, (s^-)^2)}, \quad \text{where}
$$

Please cite this article in press as: A. Kuzmin, et al., The role of the kinetic parameter in the stability of two-relaxation-time advection–diffusion lattice Boltzmann schemes, Computers and Mathematics with Applications (2010), doi:10.1016/j.camwa.2010.07.036

$$P_n(s^+,(s^-)^2) = -4(-1+\cos^2[k])(s^-)^2(4-3s^+)^2 + \big((1+\cos[k])(4+3(s^-)^2) + 3(-1+\cos[k])(s^+)^2 - 4s^+(1+2\cos[k])\big)^2, \quad \text{and}$$

$$P_d(s^+,(s^-)^2) = (-4+(s^-)^2+\cos[k]((s^-)^2-(-2+s^+)^2)+(s^+)^2)^2. \tag{B.2}$$

This yields

$$|\Omega|^2 = 1 \quad \text{if } (s^-)^2 = (s^+)^2 \quad \text{and} \quad \cos[k] = -1+s^+, \quad 0 \le s^+ \le 1. \tag{B.3}$$

The BGK model may remain stable in the limit $\Lambda_{bgk} \to 0$ only if

$$(s^-)^2 \le (s^+)^2, \quad \forall\, \alpha = 1,\dots,d. \tag{B.4}$$

This condition necessarily requires $|U_\alpha| \le \mathcal{D}^+_{\alpha\alpha}, \forall\alpha$ and for all models. Then this necessary prescribes the non-negativity of all the "moving" equilibrium weights for the minimal models (cf. relation (11)). The necessary diffusion condition $E_0 \ge 0$ completes the set of the non-negativity conditions for the minimal models.

The non-negativity conditions depend on the choice of the equilibrium weights for "full" models [23]. For instance, relations (B.4) prescribe $\{E_q \ge 0\}$ for all the coordinate links when $\{t^{(a)}_q = t^{(m)}_q\}$ and $\{\mathcal{D}^+_{\alpha\alpha} = c_e\}$. However, the strongest non-negativity condition, $U^2 \le c_e^2/d$, is then prescribed by the diagonal links. We suggest that the BGK model yields $|\Omega|^2 \to 1$ in the limit $\Lambda_{bgk} \to 0$ when $E_q^{-2} \to E_q^{+2}$ for at least one $q \in \{1,\dots,Q_m\}$ and in the limit $E_0 \to 0$. However, we are not yet aware of a generic proof.

B.2. Non-negativity lines

In this paper we often use the non-negativity conditions, or the *n-line* and the E_0-*n-line*. These are given below for an isotropic diffusion tensor ($E^{(anis)}_q = 0$). In all the cases, $c_e \in [0, c_e^{(0)}]$ and $E_0(c_e^{(0)}, U=0) = 0$. When $g^{(u)} = 0$,

$$\begin{aligned}
&\text{dDQ}(2\text{D}+1): U^2 \le c_e^2, \quad 0 \le c_e \le c_e^{(0)} = \frac{1}{d}.\\
&\text{d2Q9}^{(stan)}, \text{d2Q9}^{(unif)}: U^2 \le \frac{c_e^2}{2}, \quad 0 \le c_e \le c_e^{(0)} = \frac{1}{1+2t_c^{(m)}}.\\
&\text{d3Q15}^{(stan)}, \text{d3Q15}^{(unif)}: U^2 \le \frac{c_e^2}{3}, \quad 0 \le c_e \le c_e^{(0)} = \frac{1}{1+4t_c^{(m)}}.
\end{aligned} \tag{B.5}$$

The last two conditions are valid for all the d2Q9 and d3Q15 schemes, respectively, with the same mass and advection weights. The models with $t_c^{(m)} = 0$ and $t_c^{(a)} \ne 0$, as for $\text{d2Q9}^{(opt)}$ ($t_c^{(m)} = 0$) and $\text{d3Q15}^{(opt)}$ ($t_c^{(m)} = 0$), reduce the velocity to zero as the non-negativity condition of their coordinate links.

When $g^{(u)} = 1$ (the minimal schemes) and $g^{(u)}_{\alpha\beta} g^{(u)} = 1$ (the d2Q9 and d3Q15),

$$\text{dDQ}(2\text{D}+1): \begin{cases} d=1: (U^2 \le U_n^{2(-)}) \parallel (U^2 \ge U_n^{2(+)}), \quad 0 \le c_e \le \dfrac{1}{4}, \\ \qquad \text{and} \quad U^2 \le 1-c_e, \quad 0 \le c_e \le 1, \\ d=\{2,3\}: U^2 \le U_n^{2(-)}, \quad U_n^{2(\pm)} = \dfrac{\left(1 \pm \sqrt{1-4c_e}\right)^2}{4}, \quad 0 \le c_e \le \dfrac{1}{4}, \\ \qquad U^2 \le 1-dc_e, \quad \dfrac{1}{4} \le c_e \le \dfrac{1}{d}. \end{cases} \tag{B.6}$$

$$\begin{aligned}
\text{d2Q9}^{(stan)}: \quad & U^2 \le \frac{2}{25}\left(1-\sqrt{1-5c_e}\right)^2, \quad 0 \le c_e \le \frac{7}{36},\\
& U^2 \le 2c_e - \frac{1}{3}, \frac{7}{36} \le c_e \le \frac{11}{27}, \quad U^2 \le \frac{3-5c_e}{2}, \quad \frac{11}{27} < c_e \le \frac{3}{5}.
\end{aligned} \tag{B.7}$$

$$\begin{aligned}
\text{d2Q9}^{(unif)}: \quad & U^2 \le \frac{2}{9}\left(1-\sqrt{1-3c_e}\right)^2, \quad 0 \le c_e \le \frac{5}{16},\\
& U^2 \le 2c_e - \frac{1}{2}, \quad \frac{5}{16} \le c_e \le \frac{11}{24}, \quad U^2 \le \frac{2(2-3c_e)}{3}, \quad \frac{11}{24} < c_e \le \frac{2}{3}.
\end{aligned} \tag{B.8}$$

$$\begin{aligned}
\text{d3Q15}^{(stan)}: \quad & U^2 \le \frac{\left(\sqrt{3}-\sqrt{3-16c_e}\right)^2}{64}, \quad 0 \le c_e \le \frac{5}{27},\\
& U^2 \le 2c_e - \frac{1}{3}, \quad \frac{5}{27} \le c_e \le \frac{10}{27}, \quad U^2 \le 3-7c_e, \quad \frac{10}{27} \le c_e \le \frac{3}{7}.
\end{aligned} \tag{B.9}$$

Please cite this article in press as: A. Kuzmin, et al., The role of the kinetic parameter in the stability of two-relaxation-time advection–diffusion lattice Boltzmann schemes, Computers and Mathematics with Applications (2010), doi:10.1016/j.camwa.2010.07.036

$$\mathrm{d3Q15}^{(unif)}: \quad U^2 \le \frac{\left(\sqrt{3}-\sqrt{3-8c_e}\right)^2}{16}, \quad 0 \le c_e \le \frac{9}{25}, \qquad U^2 \le 2c_e - \frac{3}{5}, \quad \frac{9}{25} \le c_e \le \frac{34}{75}, \quad U^2 \le \frac{5}{3} - 3c_e, \quad \frac{34}{75} \le c_e \le \frac{5}{9}. \tag{B.10}$$

These solutions are particular cases [23], Appendix B, where they are built for general weights $\{t_q^{(m)}, t_q^{(a)}, t_q^{(u)}\}$ and also in the case $g^{(u)} = 1, g_{\alpha\beta}^{(u)} g^{(u)} = 0$. The non-negativity domain generally increases when the cross-diagonal numerical diffusion is cancelled, $g_{\alpha\beta}^{(u)} g^{(u)} = 1$.

Appendix C. Numerical stability analysis

We look for $\{\Omega_q\}$, the set of Q roots of the characteristic equation of the TRT scheme with the equilibrium distribution in the form (3):

$$\begin{aligned} &\det|L - \Omega I| = 0, \quad \text{where} \\ &L = K^{(-1)}[I + C], \quad K_{ij}^{(-1)} = \exp(-\mathrm{i}k_i)\delta_{ij}, \quad k_i = \vec{k}\cdot\vec{c}_i, \\ &C_{ij} = \lambda^+\left(\frac{\delta_{ij}+\delta_{\bar{i}\bar{j}}}{2} - E_i^+\right) + \lambda^-\left(\frac{\delta_{ij}-\delta_{\bar{i}\bar{j}}}{2} - E_i^-\right), \quad \{i,j\} = 0,\ldots,Q_m. \end{aligned} \tag{C.1}$$

The (equilibrium) components of the matrix **C** are obtained using $s = \sum_{q=0}^{Q_m} f_q$ in relation (3). The linear stability is guaranteed in the von Neumann sense when all $|\Omega_q| \le 1$. The following 3D form is adapted to represent the velocity vector $\vec{U}$ and the wavevector $\vec{k}$ (with $U = |\vec{U}|$ and $k = |\vec{k}|$):

$$\begin{aligned} &\vec{U} = \{U_x, U_y, U_z\} = U\{\cos\psi\sin\alpha, \sin\psi\sin\alpha, \cos\alpha\}, \\ &\vec{k} = \{k_x, k_y, k_z\}, \quad \text{with} \\ &k_x = k\{\cos\psi\cos\theta\sin\alpha - \cos\phi\cos\psi\cos\alpha\sin\theta + \sin\phi\sin\psi\sin\theta\}, \\ &k_y = k\{\cos\theta\sin\psi\sin\alpha - \sin\phi\cos\psi\sin\theta - \cos\phi\cos\alpha\sin\psi\sin\theta\}, \\ &k_z = k\{\cos\alpha\cos\theta + \cos\phi\sin\alpha\sin\theta\}. \end{aligned} \tag{C.2}$$

We vary $\vec{k}$ with respect to $\vec{U}$. The two vectors are parallel when both θ and ϕ are equal to zero. In two and three dimensions, we typically use $\theta \in [0, \pi, \pi/8]$ and $\phi \in [0, \pi, \pi/8]$, with $k \in \{0, \sqrt{d}\pi, \sqrt{d}\pi/72\}$. In particular, $\vec{U} = U\{1,0,0\}$ when $\alpha = \pi/2$ and $\psi = 0$, then $\vec{U} = \frac{U}{\sqrt{2}}\{1,1,0\}$ when $\alpha = \pi/2$ and $\psi = \pi/4$, and finally, $\vec{U} = \frac{U}{\sqrt{3}}\{1,1,1\}$ when $\alpha = \arccos(\sqrt{3}/3)$ and $\psi = \pi/4$. In two dimensions we set $\alpha = \frac{\pi}{2}$ and typically use $\psi \in [0, \pi, \pi/8]$, with about 50–200 points for $|U|$. In three dimensions, we typically use $\psi \in [0, \pi/4, \pi/32]$, $\alpha \in [\arccos(\sqrt{3}/3), \pi/2]$, with eight points per interval and about 20–40 points for $|U|$. We output as *unstable* those pairs (c_e, U^2) where there is a root Ω of characteristic equation (C.1) such that $|\Omega| \ge 1 + \epsilon$ with $\epsilon = 10^{-14}$; $\{\Omega_q\}$ is computed with the help of the CLAPACK library.

References

[1] Y. Qian, D. d'Humières, P. Lallemand, Lattice BGK models for Navier–Stokes equation, Europhys. Lett. 17 (1992) 479–484.
[2] F.J. Higuera, J. Jiménez, Boltzmann approach to lattice gas simulations, Europhys. Lett. 9 (1989) 663–668.
[3] F.J. Higuera, S. Succi, R. Benzi, Lattice gas dynamics with enhanced collisions, Europhys. Lett. 9 (1989) 345–349.
[4] D. d'Humières, Generalized lattice-Boltzmann Equations. AIAA Rarefied Gas Dynamics: Theory and Simulations, in: Progress in Astronautics and Aeronautics, vol. 59, 1992, pp. 450–548.
[5] D. d'Humières, I. Ginzburg, M. Krafczyk, P. Lallemand, L.-S. Luo, Multiple-relaxation-time lattice Boltzmann models in three dimensions, Philos. Trans. R. Soc. Lond. A 360 (2002) 437–451.
[6] I. Ginzburg, Equilibrium-type and link-type lattice Boltzmann models for generic advection and anisotropic-dispersion equation, Adv. Water Res. 28 (2005) 1171–1195.
[7] I. Ginzburg, Lattice Boltzmann modeling with discontinuous collision components. Hydrodynamic and advection–diffusion equations, J. Stat. Phys. 126 (2007) 157–203.
[8] X. Zhang, A.G. Bengough, L.K. Deeks, J.W. Crawford, I.M. Young, A lattice BGK model for advection and anisotropic dispersion equation, Adv. Water Res. 25 (2002) 1–8.
[9] X. Zhang, A.G. Bengough, L.K. Deeks, J.W. Crawford, I.M. Young, A novel three-dimensional lattice Boltzmann model for solute transport in variably saturated porous media, Water Resour. Res. 38 (2002) 1167–1177.
[10] Y. Li, P. Huang, A coupled lattice Boltzmann model for advection and anisotropic dispersion problem in shallow water, Adv. Water Res. 31 (12) (2008) 1719–1730.
[11] I. Ginzburg, D. d'Humières, Lattice Boltzmann and analytical modeling of flow processes in anisotropic and heterogeneous stratified aquifers, Adv. Water Res. 30 (2007) 2202–2234.
[12] B. Servan-Camas, F.T.C. Tsai, Saltwater intrusion modeling in heterogeneous confined aquifers using two-relaxation-time lattice Boltzmann method, J. Comput. Phys. 228 (2009) 236–256.
[13] R.G.M. van der Sman, M.H. Ernst, Diffusion lattice Boltzmann scheme on an orthorhombic lattice, J. Stat. Phys. 94 (1–2) (1999) 203–217.

Please cite this article in press as: A. Kuzmin, et al., The role of the kinetic parameter in the stability of two-relaxation-time advection–diffusion lattice Boltzmann schemes, Computers and Mathematics with Applications (2010), doi:10.1016/j.camwa.2010.07.036

[14] P. Lallemand, L.-S. Luo, Theory of the lattice Boltzmann method: dispersion, dissipation, isotropy, Galilean invariance, and stability, Phys. Rev. E 61 (2000) 6546–6562.
[15] I. Ginzburg, Consistent lattice Boltzmann schemes for the Brinkman model of porous flow and infinite Chapman–Enskog expansion, Phys. Rev. E 77 (0666704) (2008) 1–12.
[16] D. d'Humières, I. Ginzburg, Viscosity independent numerical errors for lattice Boltzmann models: from recurrence equations to magic collision numbers, Comput. Math. Appl. 58 (5) (2009) 823–840.
[17] I. Ginzburg, Magic recipes for lattice Boltzmann modeling of micro and macro flow, Habilitation Thesis, University Paris VI, 2009.
[18] I. Ginzburg, F. Verhaeghe, D. d'Humières, Two-relaxation-time lattice Boltzmann scheme: about parametrization, velocity, pressure and mixed boundary conditions, Commun. Comput. Phys. 3 (2008) 427–478.
[19] M. Rheinländer, Stability and multiscale analysis of an advective lattice Boltzmann scheme, Prog. Comput. Fluid Dyn. 8 (1–4) (2008) 56–68.
[20] S. Suga, Numerical schemes obtained from lattice Boltzmann equations for advection–diffusion equations, Internat. J. Modern Phys. C 17 (11) (2006) 1563–1577.
[21] B. Servan-Camas, F.T.C. Tsai, Non-negativity and stability analysis of lattice Boltzmann method for advection–diffusion equation, J. Comput. Phys. 228 (2009) 236–256.
[22] B. Servan-Camas, F.T.C. Tsai, Lattice Boltzmann method for two relaxation times for advection–diffusion equation: third order analysis and stability analysis, Adv. Water. Res. 31 (2008) 1113–1126.
[23] I. Ginzburg, D. d'Humières, A. Kuzmin, Optimal stability of advection–diffusion lattice Boltzmann models with two relaxation times for positive/negative equilibrium, J. Stat. Phys. 139 (6) (2010) 1090–1143. doi:10.1007/s10955-010-9969-9.
[24] A.C. Hindmarsch, P.M. Grescho, D.F. Griffiths, The stability of explicit time-integration for certain finite difference approximation of the multi-dimensional advection–diffusion equation, Internat. J. Numer. Methods Fluids (4) (1984) 853–897.
[25] J.J.H. Miller, On the location of zeros of certain classes of polynomials with application to numerical analysis, J. Inst. Math. Appl. 8 (1971) 397–406.
[26] S. Wolfram, Software package Mathematica 6.

Please cite this article in press as: A. Kuzmin, et al., The role of the kinetic parameter in the stability of two-relaxation-time advection–diffusion lattice Boltzmann schemes, Computers and Mathematics with Applications (2010), doi:10.1016/j.camwa.2010.07.036